IEEE Access
Multidisciplinary | Rapid Review | Open Access Journal

Received December 31, 2020, accepted February 10, 2021, date of publication February 22, 2021, date of current version March 19, 2021.

*Digital Object Identifier 10.1109/ACCESS.2021.3061250*

# A Comprehensive Study of Optical Frequency Domain Reflectometry

**CHANGSHUO LIANG[1], QING BAI[1], MIN YAN[1], YU WANG[1], HONGJUAN ZHANG[2], AND BAOQUAN JIN[1,3]**

[1]Key Laboratory of Advanced Transducers and Intelligent Control Systems (Ministry of Education and Shanxi Province), College of Physics and Optoelectronics, Taiyuan University of Technology, Taiyuan 030024, China
[2]College of Electrical and Power Engineering, Taiyuan University of Technology, Taiyuan 030024, China
[3]State Key Laboratory of Coal and CBM Co-mining, Jincheng 048000, China

Corresponding author: Baoquan Jin (jinbaoquan@tyut.edu.cn)

This work was supported in part by the National Natural Science Foundation of China under Grant 61975142 and Grant 62005190, in part by the Coal-Bed Methane Joint Research Fund of Shanxi Province, China, under Grant 2015012005 and Grant 2016012011, and in part by the Natural Science Foundation of Shanxi Province, China, under Grant 201901D211072.

**ABSTRACT** Optical frequency domain reflectometry (OFDR) is a kind of distributed optical fiber sensors (DOFS) which has attracted an increasing amount of research attention. The OFDR sensor has a high spatial resolution and large dynamic range, which makes it useful in a large amount of sensing scenarios. In this paper, we will provide a review of the recent advances in OFDR. We introduce the sensing principles and progress for performance improvement of the system. We also cover the applications of OFDR-based sensing system, including sensing of temperature, strain, vibration, pressure, magnetic field, refractive index, radiation, 3D-shape, gas, gas flow rate, and so on.

**INDEX TERMS** Distributed optical fiber sensors, frequency modulated continuous wave (FMCW), optical fiber sensors, optical frequency domain reflectometry (OFDR), phase noise compensation, Rayleigh backscattering.

## I. INTRODUCTION

Since the emergence of the optical fiber in the 1970s [1], it was widely used in high speed and long range communication as a reliable information transmission medium. In the meantime, distributed optical fiber sensing (DOFS) technology arose with the development of the fiber optic communication. Due to optical fiber's competence of acting simultaneously as the sensing elements and the sensing data transmission medium and its advantages in sensing range, spatial resolution etc., it has attracted the attention of a large number of researchers. A growing number of optical fiber sensors were developed utilizing different optical effects of optical fiber, including Rayleigh, Brillouin, and Raman backscattering [2], [3].

DOFS is achieved by injecting laser referred to as test light into the fiber under test (FUT) and analyzing different parameters of the backscattering signal. The backscattering signal can be analyzed in time domain and frequency domain. The Rayleigh backscattering effect was firstly analyzed in time domain for attenuation and imperfections sensing of the optical fiber, which was named optical time domain reflectometer (OTDR) [4]. By injecting a pulse light signal as the test light and analyzing the Rayleigh backscattering, OTDR can measure attenuation and imperfection of FUT reliably. The technology was then extended to polarization-OTDR (POTDR), phase-sensitive OTDR ($\varphi$-OTDR) and coherent OTDR (COTDR) for vibration sensing [5], [6]. The Raman backscattering is utilized in Raman OTDR (ROTDR) for distributed temperature sensing as it is sensitive to the temperature change along the FUT [7]. The Brillouin backscattering is related to both the temperature and strain [8], [9]. Thus, it is used in Brillouin OTDR (BOTDR) and Brillouin optical time domain analysis (BOTDA) for temperature and strain measurement [10], [11]. The spatial resolution and the signal-to-noise-ratio (SNR) of time domain DOFS is dependent on the width of the test pulse signal in the opposite way. On one hand, the width needs to be decreased to improve the spatial resolution of the system. On the other hand, however, the decrease of the width can lead to a deterioration of the SNR, which limits the sensing range. Therefore, the spatial resolution and SNR meet a trade-off, which is a main

The associate editor coordinating the review of this manuscript and approving it for publication was Maged Abdullah Esmail.

drawback of the time domain DOFS. To rise above the trade-off comes the frequency domain DOFS.

The frequency domain DOFS has been given tremendous attention for its high spatial resolution and large dynamic range. In 1981, Eickhoff *et al.* originally analyzed Rayleigh backscattering in frequency domain for DOFS, which was named optical frequency domain reflectometer (OFDR) [12]. The system consists of a tunable laser source (TLS) to generate continuous laser whose optical frequency is tuned linearly in time, and an interferometer with a measurement arm and a reference arm. The frequency-sweeping laser from the TLS is injected into the interferometer and the output of the interferometer is analyzed for sensing parameters demodulation. OFDR was firstly utilized to test the attenuation and imperfections of the FUT, which was similar to OTDR. The system achieved a millimeter-level spatial resolution at a short range as an order of tens to hundreds of meters. And the sensing range was improved to an order of hundreds of kilometers with the development of the narrow linewidth TLS along with solutions of OFDR phase noise. The sensing parameters were extended to strain and temperature. In 1998, Froggatt *et al.* firstly utilized OFDR system for strain and temperature measurement [13]. The Rayleigh backscattering spectra (RBS) shifts was analyzed for strain and temperature sensing. The system has a millimeter-level spatial resolution over 30 cm FUT. And the sensing parameters in OFDR-based sensing systems have been extended to temperature, strain, vibration, pressure, magnetic field, refractive index, radiation, 3D-shape, gas, gas flow rate etc.

In this paper, we introduce the sensing mechanisms and demodulation principles of the OFDR based sensing system. We review the methods for performance improvement of the OFDR system including TLS performance enhancement, phase noise compensation, polarization-induced fading solution and demodulation algorithm improvement. We also summarize the applications of OFDR-based sensing system including temperature, strain, vibration, pressure, magnetic field, refractive index, radiation, 3D-shape, gas, gas flow rate sensing with the use of conventional types of optical fibers and special optical fibers.

## II. PRINCIPLE OF OFDR

OFDR utilizes Rayleigh backscattering for distributed measurement of several parameters along FUT. The measured parameters include attenuation, imperfection, temperature and strain. In this section, we introduce the 2 main aspects of OFDR sensing principle, the interference of the main interferometer principle and the signal demodulation principle.

### A. PRINCIPLE OF OFDR INTERFERENCE

The principle of OFDR is based on utilizing interferometer and swept-frequency light to generate beating signals. Fig. 1 shows the basic configuration of an OFDR system utilizing a Mach-Zehnder interferometer. The swept-frequency light from the TLS is split into the reference light and the measurement light through coupler A. The reference light

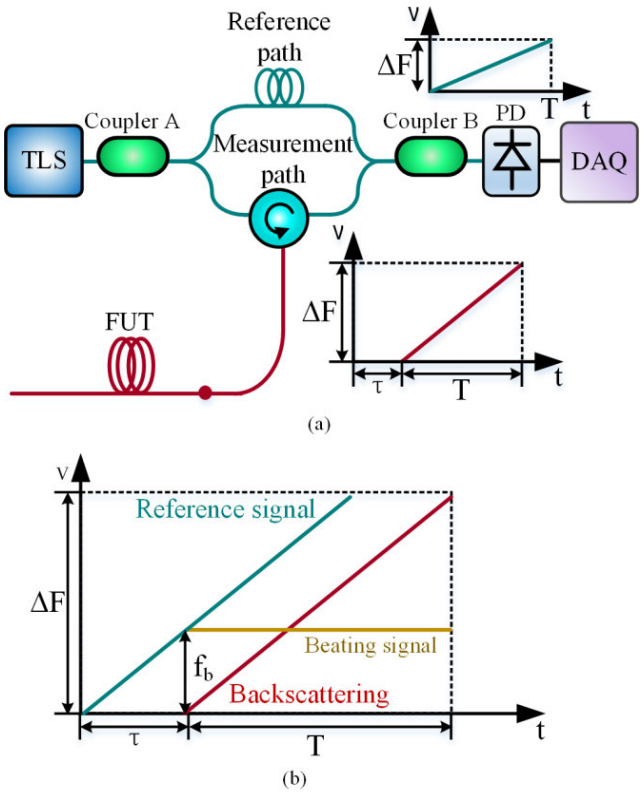


**FIGURE 1.** (a) OFDR system configuration, (b) beating signal between reference and backscattering signals under linearly optical frequency tuning condition.

is transferred through the reference path with a given optical distance into coupler B, while the measurement light is transferred through the measurement path into the FUT which returns the backscattering light. Coupler B then recombine the reference light with the backscattering light and a beating between these two lights occurs in the photo diode (PD). The beating signal is then analyzed to demodulate the shift of the physical parameters with its location.

In more detail, the beating signal is from beating two light signals out of two different paths. One light signal $E_s(t)$ is the backscattering light from the FUT, which contains the Rayleigh backscattering light and the Fresnel reflection light. The other light signal $E_r(t)$ is the reference light from the reference path. Assuming that the TLS has a linear optical frequency tuning rate $\gamma$, the reference signal $E_r(t)$ can be written as [14]:

$$E_r(t) = E_0 \exp\{j[2\pi f_0 t + \pi\gamma t^2 + e(t)]\}. \quad (1)$$

where $E_0$ is the amplitude of the reference signal. $f_0$ is the initial optical frequency. $e(t)$ is the phase noise. The backscattering signal $E_s(t)$ can be written as:

$$E_s(t) = \sqrt{R(\tau)}E_0 \exp\{j[2\pi f_0(t-\tau) + \pi\gamma(t-\tau)^2 + e(t-\tau)]\}. \quad (2)$$

where $R(\tau)$ is the reflectivity attenuation of FUT related to the time delay $\tau$. The beating signal $I(t)$ from the interference between $E_r(t)$ and $E_s(t)$ can be written as

$$I(t) = 2\sqrt{R(\tau)}E_0^2 \cos\{2\pi[f_0\tau + \gamma\tau t + \frac{1}{2}\gamma\tau^2 + e(t) - e(t-\tau)]\}. \quad (3)$$

The last phase term $e(t) - e(t-\tau)$ is the phase noise in the beating signal. The frequency of the beating signal $f_b = \gamma\tau$. It is linear related to the time delay $\tau$, and thus linear related to the distance between the backscatter point and the start point of FUT. As a conclusion, the beating frequency $f_b$ represents the location of the backscatter point of FUT. By deriving and analyzing different frequency segments of the beating signal, signals from different locations of the FUT can be interrogate separately.

### B. PRINCIPLE OF OFDR SIGNAL DEMODULATION

The Rayleigh backscattering is caused by random fluctuations of the refractive index along the FUT. For a given FUT, the scatter amplitude is a static function of distance along the fiber. And it can be modeled as a long, weak FBG with random but static period. Changes of the physical parameters (temperature or strain) along the FUT can cause shifts of the local period, and thus cause shifts of the local RBS. The RBS shifts along the FUT can be found by a cross-correlation between beating signals of the same FUT under different temperature or strain situations. And a distributed temperature or strain sensing can be achieved by analyzing the RBS shift along the FUT. The signal processing procedure shown in Fig. 2 is as follows [15]:

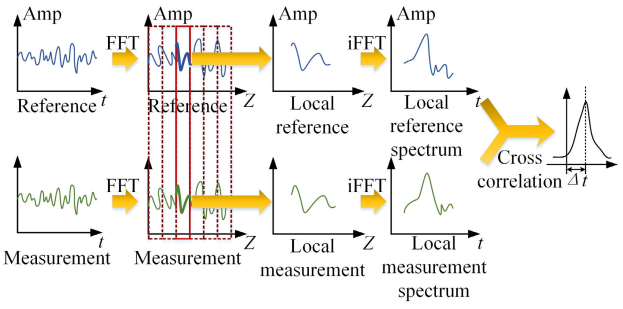


**FIGURE 2. Demodulation procedure of RBS shifts in OFDR system.**

*Step 1:* Making a measurement to the given FUT with ambient temperature and no strain variation. Save the beating signal as the reference signal in time domain.

*Step 2:* Making another measurement to the same FUT as step 1, but with temperature or strain variation applied to the fiber. Save the beating signal as the measurement signal in time domain.

*Step 3:* Converting both the reference signal and the measurement signal from time domain to frequency domain by a fast Fourier transform (FFT). The frequency domain signals are also spatial domain signal as frequencies of the beating signals are linear related to the scatter locations of the signals.

*Step 4:* Dividing the whole FUT into several interval length segments utilizing a sliding window with a length of $\Delta X$ which holds N data points of local beating signals. The effective sensing spatial resolution $\Delta X$ can be written as:

$$\Delta X = N\Delta Z. \quad (4)$$

where:

$$\Delta Z = c/2n\Delta\upsilon. \quad (5)$$

where $\Delta Z$ is the spatial resolution of a single data point, n is the refractive index of FUT, $\Delta\upsilon$ is the optical tuning range of the TLS.

*Step 5:* Converting each local beating signal interval back to time domain by an inverse FFT. The result is the reference and measurement RBS of each interval along the FUT.

*Step 6:* Performing a cross-correlation of the reference and the measurement RBS of each interval. The shifts in the correlation peak represent the RBS shifts of each interval along the FUT, which are linear related to the changes of the sensing parameters such as temperature or strain.

Analyzing RBS shift data of each interval along the FUT, the temperature or strain changes in each interval can be acquired.

### C. STRAIN AND TEMPERATURE CALIBRATION

As is mentioned in II.B, the Rayleigh backscattering signal of FUT can be modeled as a long, weak FBG along the FUT. Changes in effective line spacing and effective refraction index cause shifts to the RBS. The wavelength shift, $\Delta\lambda$, or frequency shift, $\Delta\nu$, of the Rayleigh backscattering signal shows the same response with FBG to the temperature change, $\Delta T$, or strain parallel to the fiber axis, $\varepsilon$ [16]:

$$\frac{\Delta\lambda}{\lambda} = -\frac{\Delta\nu}{\nu} = K_T\Delta T + K_\varepsilon\varepsilon. \quad (6)$$

where $K_T$ is the temperature coefficient, $K_\varepsilon$ is the strain coefficient.

The temperature and strain coefficients vary in different types of fiber. For a particular fiber type, these coefficients can be calibrated by recording the RBS shift for a given temperature or strain shift. The temperature coefficient has typical values of $0.55 \times 10^{-6}\ ^\circ C^{-1}$ and $6.1 \times 10^{-6}\ ^\circ C^{-1}$ for Ge-doped silica core fibers. And the strain coefficient has a typical value of 0.787.

## III. ENHANCEMENTS OF THE OFDR SENSING SYSTEM PERFORMANCE

OFDR system is based on the frequency sweeping laser from the TLS and the interference between the Rayleigh backscattering and the reference light. The performance of OFDR is impaired mostly by problems occur in the TLS and the interferometer, such as the nonlinear tuning problem of the TLS and polarization-induced fading problem of the interferometer. In this section, we reviewed solutions to the problems in OFDR for performance enhancements, including TLS tuning linearity improvement, nonlinear phase noise

compensation and polarization diversity detection. We also introduced modifications of the signal processing method and means of SNR improvement.

### A. TLS TUNING LINEARITY IMPROVEMENT IN OFDR SYSTEM

In OFDR, the beating signals collected in time domain are transformed into frequency domain so as to make different frequency segments of the signals to match local Rayleigh backscattered light from different distances of the FUT. Namely, the frequency resolution of the beating signals is a decisive factor of the system spatial resolution. Due to the mechanism of the conventional TLS, the frequency sweeping laser from the TLS has a nonlinear problem. The frequency tuning rate varies with time, which results in a nonlinear frequency sweeping of the TLS. The nonlinear frequency sweeping makes the energy of the Rayleigh backscattering light spread, which results in a widen of the reflection peaks in the frequency domain. The results are a decrease of the refection intensity and a worsen of the spatial resolution [17]–[20]. Fig. 3 shows the beating signals between the measurement light and the reference light under the condition of TLS nonlinear tuning. As the tuning rate varies with time, the beat frequencies are not constants with other frequencies generated when sampled with a constant spacing in time. The nonlinear tuning of TLS results in the phase noise of the signal, which impairs the demodulation quality and the system performance.

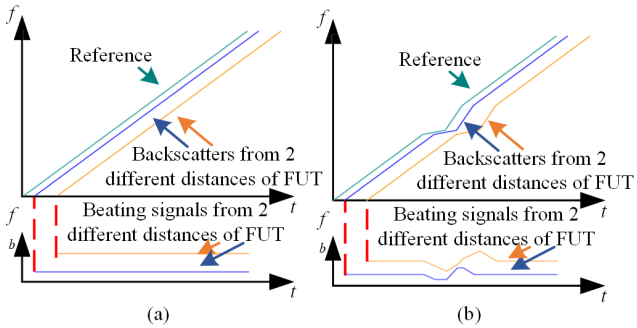


**FIGURE 3.** Beating signals from 2 different distances of FUT with (a) linearly optical frequency tuning TLS and (b) nonlinearly optical frequency tuning TLS.

In general, the suppression of the phase noise caused by the TLS nonlinear tuning is one of the keys to improve the sensing performance such as spatial resolution and sensing range. The solutions can be divided into 2 kinds. The one focuses on improving the frequency tuning linearity of the TLS, while the other pays attention to compensation of the phase noise caused by the TLS.

As for TLS tuning linearity improvement, the frequency sweeping continuous laser can be generated in 2 kinds of laser sources. The one is the internal modulation TLS, which generates the frequency sweeping laser directly with the frequency controlled by adjusting the cavity parameters of the laser source. And the other is the external modulation TLS, which generates a frequency stabilized laser and modulate it using optical modulator to make the frequency sweeping laser [21]. In this section, we reviewed the 2 types of approaches to enhance the tuning linearity of the TLS. The first is based on the internal modulation TLS and the second is based on the external modulation TLS.

#### 1) INTERNAL MODULATION TLS METHOD

The internal modulation TLS based method modifies the TLS using different approaches for the improvement of the tuning rate, tuning linearity and laser linewidth.

In terms of TLS tuning linearity enhancement, Fujiwara *et al.* suppressed the thermal wavelength drift in a super-structure grating distributed Bragg reflector (SSG-DBR) laser for a linearly tuning laser by involving a thermal drift compensation (TDC) waveguide into the laser source [22]. Boukari *et al.* studied the chirp pattern induced by direct modulated distributed feedback (DFB) laser in theory and through a software simulation and analyzed the variation of the optical frequency in time [23], [24]. The study shows promise in a linear tuning DFB laser source configuration. Deng *et al.* analyzed and modeled the nonlinearity of the external cavity laser diode using a system identification method [25]. The relationship between drive current and laser frequency was deduced. By adjusting the drive current in time, a linear tuning laser was achieved, with a determination coefficient ($R^2$) of 0.99975. And an OFDR system using the above-mentioned TLS showed a standard localization deviation which reduced below 7 $\mu$m and a relative measurement residual error of 75 ppm. Tkachenko *et al.* proposed an OFDR system using a simple single-frequency fiber laser with self-scanning [26]. The frequency of the laser was tuned linearly with the pulse number change, which requires no other actively tuned elements. The OFDR system achieved a sensitivity of around −80 dB on a 9 m long FUT.

In terms of a high-speed tuning laser, Golubovic *et al.* utilized a cw chromium-doped forsterite laser, which can sweep a tuning range of 1200 to 1275 nm in less than 500 $\mu$s, and achieved a frequency-domain ranging with a scan rate of 2 kHz and a spatial resolution of 15 $\mu$m [27]. Ndiaye studied the performance of a frequency-shifted feedback laser (FSFL) and utilized it in an OFDR system and achieved a measurement time of 2 ms with distance accuracies better than 25 $\mu$m [28]. Nakemura *et al.* used a FSFL as the TLS in an OFDR system and achieved a tuning rate faster than 100 PHz/s, which contributed to a 18.5 km sensing range OFDR with a spatial resolution of 20 mm [29].

In terms of a narrow linewidth laser, Oberson *et al.* presented an OFDR system with a TLS which compose of a single-mode erbium-doped fiber laser and a piezoelectric component to control the frequency by stretching the fiber [30]. The linewidth of the laser is around 10 kHz and the OFDR system using the proposed TLS achieved a −110 dB sensitivity and 80 dB dynamic range. The measurement spatial resolution is 16 cm at a distance of 150 m and sub centimeter at a distance of 5 m.

A brief list of the OFDR system based on different kinds of modified internal modulation TLS with their performance summary is shown in Table 1.

**TABLE 1. Performance summary of modified internal modulation TLS based OFDR system.**

| Method | System Achievement | Value |
|---|---|---|
| SSG-DBR laser with TDC[22] | Wavelength error | 5 GHz |
| DFB laser[23, 24] | Tuning rate | 230 GHz/μs |
| System identification method[25] | Standard localization deviation | < 7 μm |
| | Relative measurement residual error | 75 ppm |
| Self- scanning laser[26] | Sensitivity | -80 dB |
| | Sensing range | 9 m |
| Cw laser[27] | Tuning rate | 2 kHz |
| | Spatial resolution | 15 μm |
| FSFL[28] | Measurement time | 2 ms |
| | Distance deviation | < 25 μm |
| FSFL[29] | Tuning rate | > 100 PHz/s |
| | Sensing range | 18.5 km |
| | Spatial resolution | 20 mm |
| Piezoelectric tuning control[30] | Sensing range | 150 m |
| | Spatial resolution | 16 cm |

### 2) EXTERNAL MODULATION TLS METHOD

He *et al.* proposed an OFDR system with external modulation based TLS which generates a tuning frequency comb, and presented the delay shift averaging (DSAV) scheme which utilizes the tuned frequency comb for fading noise suppression [31]. The external modulation TLS consists of a conventional frequency stabilized fiber laser, a phase modulator with an intensity modulator for frequency comb forming, and a single sideband modulator (SSBM) for frequency sweep tuning of the comb. The system also added a tunable delay line (TDL) at the reference arm in order to obtain multiple OFDR signals at different optical delay. The OFDR signals are averaged with the method of DSAV to reduce the fading noise.

Li *et al.* used a recirculating frequency shifter (RFS) as the external frequency modulator in a conventional OFDR to broaden the frequency sweeping range of the TLS [32]. The RFS shown in Fig. 4 consists of an optical loop with an I/Q modulator which is driven by a radio frequency synthesizer (RF). The frequency stabilized laser from the TLS is injected into the optical loop and tuned with the I/Q modulator multiple times, which generates an optical frequency comb as a result. The high order sideband is derived from the frequency comb by band pass filter (BPF), which act as the frequency sweeping laser. The RFS achieved an optical frequency sweeping range which is 12 times broadened. And the OFDR system with the broadened sweeping range laser has a 0.97 cm spatial resolution over 710 m sensing range. In addition, Du *et al.* investigated the combination of high-order SSBM with RFS [33]. The high order SSB can enlarge the frequency range between the frequency comb teeth, and thus extend the frequency sweeping range.

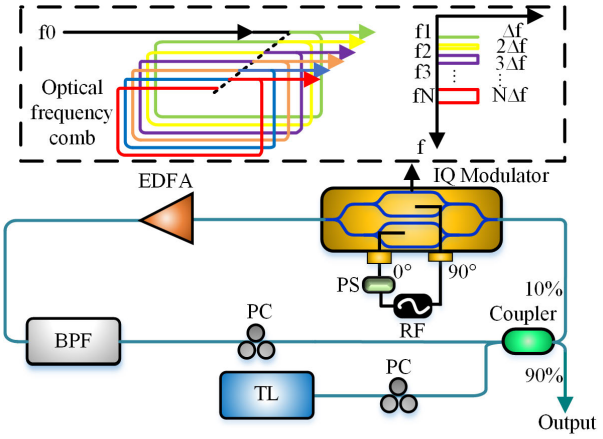


**FIGURE 4. Configuration of RFS system with SSBM.**

Badar *et al.* utilized four wave mixing (FWM) to increase the frequency tuning range, so as to improve the spatial resolution [34]. Two optical frequency sidebands generated by a double sideband with suppress carrier (DSB-SC) modulator act as two separate light source and other two frequency bands were created from beating of the two light source. With two light source bands and two beating frequency bands, the FWM occurred which generated a tuning laser with 3 times enlarged frequency tuning range. And the OFDR system with FWM technology achieved a spatial resolution about 10 cm on an FUT with 10 km length with 400 MHz frequency sweep span. Fan *et al.* combined the FWM with high order sideband to further extend the tuning range [35]. The sweeping laser source used injection lock technique to filter out the 8th order sidebands as the two separated light sources. And the FWM was then occurred to the 8th order sidebands for an even larger sweeping range. With this combination method, the OFDR system obtained a 4.2 mm spatial resolution over 10 km measurement range with the RF signal sweep range of 3.3 GHz.

A brief list of the OFDR system based on different kinds of modified external modulation TLS with their performance summary is shown in Table 2.

**TABLE 2. Performance summary of modified external modulation TLS based OFDR system.**

| Method | Spatial Resolution | Sensing Range |
|---|---|---|
| DSAV[31] | 5 cm | 300 m |
| RFS[32] | 0.97 cm | 710 m |
| DSB-SC + FWM[34] | 10 cm | 10 km |
| high-order SSBM + FWM [35] | 4.2 mm | 10 km |

## B. NONLINEAR PHASE NOISE ISSUE COMPENSATION IN OFDR SYSTEM

Improving the tuning linearity of the TLS can mitigate the nonlinear phase noise problem significantly, but with high cost for TLS modification. Another solution of nonlinear phase noise problem is phase noise compensation, which

works to extract and compensate the phase noise in signals. We mainly reviewed 3 types of nonlinear phase noise compensation methods, frequency-sampling method, software algorithms compensation method, and short-tuning-range-based method. We also reviewed some other kinds of nonlinear phase compensation methods.

### 1) FREQUENCY-SAMPLING METHOD

When the TLS tuning rate is not constant, the signals sampled at even time intervals are not sampled at even frequency intervals. In frequency-sampling method, the sampling is performed at even frequency intervals instead of time [36]. The system configuration shown in Fig. 5 consists of a main Michelson-type interferometer for OFDR sensing, and an auxiliary Mach-Zehnder interferometer for frequency-sampling trigger. The DAQ is triggered by an external clock from the auxiliary interferometer. In more detail, the times of the zero crossing points of the signal from the auxiliary interferometer are the times that the DAQ sampling the signal from the main interferometer. This method is reliable and sufficient for nonlinearly tuning compensation within the sensing range. However, the main drawback of the method is that the sensing range is limited by the length of the delay fiber in the auxiliary interferometer due to Nyquist Law, which makes the sensing range short [36], [37].

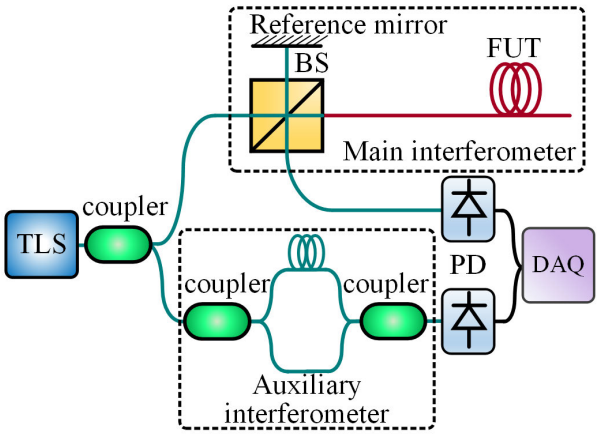


**FIGURE 5.** Configuration of OFDR system using frequency-sampling method.

In order to extend the sensing range restricted by the length of the delay fiber in the auxiliary interferometer, Koichi Iiyama *et al.* presented an OFDR system with a modified auxiliary interferometer [38]. The system with configuration shown in Fig. 6 utilized a PLL circuit (PLL-IC) in the auxiliary interferometer to electronically frequency-multiply the trigger signals from the auxiliary interferometer. In the auxiliary interferometer, as the trigger signals are frequency-multiplied, an interferometer with a given length of delay fiber can generate trigger signals with higher frequencies, which corresponds to a longer sensing range. With this method, the measurement range can be experimentally extended by a factor of 20 with high spatial resolution kept.

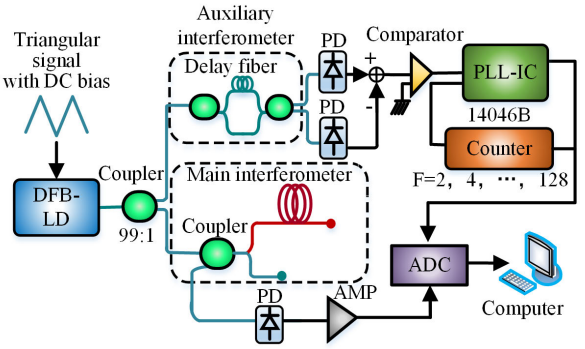


**FIGURE 6.** Configuration of OFDR system using frequency-sampling method with frequency-multiplied trigger signal.

### 2) SOFTWARE ALGORITHMS COMPENSATION METHOD

Software algorithms compensation method shares the similar hardware system with the frequency-sampling method, which contains a main interferometer and an auxiliary interferometer. In this type of method, the auxiliary interferometer is utilized for the phase information acquisition of the TLS. The signal from the auxiliary interferometer is collected and analyzed to find out the phase information of the TLS. Based on the acquired phase information, several kinds of software algorithms are used to compensate the phase noise.

One kind of the software algorithms is the re-sampling method. In this kind of method, the signals from the main interferometer are re-sampled based on the TLS phase information using interpolation algorithms. In more detail, the beating signal from the auxiliary interferometer is sampled along with signal from the main interferometer at even time intervals, the phase information of the TLS is obtained through Hilbert Transformation of the auxiliary signal [39], [40] or through differential of the normalized auxiliary signal [17]. From the phase information of the TLS, the frequencies of the tuning light at every sampling point can be deduced. If the tuning rate of the TLS is a constant, the data points sampled at even time intervals are also at even frequency intervals. However, as the presence of the nonlinear tuning, the tuning rate of TLS is not a constant, so the data points sampled at even time intervals are interpolated and re-sampled at even frequency intervals. The interpolation methods can be chosen from linear interpolation [41] and cubic spline interpolation [17], [40], [41]. The re-sampled signals are then processed similarly as the sampled data to demodulate the strain and temperature along the FUT.

Non-uniform FFT (NUFFT) is another kind of re-sampling method utilizes NUFFT instead of interpolation [42]. The data processing procedure is shown in Fig. 7. Through NUFFT method, the original signal $x(\upsilon_n)$ sampled at uneven frequency intervals is convolved with a Gaussian window function $\omega(\upsilon_n)$, the result of which is then re-sampled at even frequency intervals to get $x(\upsilon_k)$. Transform $x(\upsilon_k)$ and $\omega(\upsilon_n)$ into frequency domain signals $X_G(z_n)$ and $W(z_n)$ by FFT. And $X_G(z_n)$ is then deconvoluted by $W(z_n)$ to get $X_{app}(z_n)$.

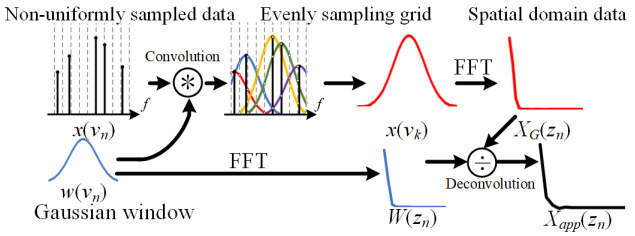


**FIGURE 7.** NUFFT signal processing procedure.

$X_{app}(z_n)$ is the re-sampled frequency domain signal which is processed similarly as the frequency domain sampled data to demodulate the strain and temperature along the FUT.

Fumihiko *et al.* presented concatenately generated phase (CGP) method to calculate the phase of every sample points of the signal [19], [43], [44]. The method extends the sensing range beyond the coherence length. The method utilized the similar OFDR system configuration, which consists of a main interferometer and an auxiliary interferometer. The reference delay of the auxiliary interferometer is defined as $\tau_{ref}$. The signals from the auxiliary interferometer with the time delay of $N\tau_{ref}$ (N: integer) have the phase term $X_N(t)$ which meets the following relationship:

$$X_N(t) = \sum_{n=0}^{N-1} X_1(t - n\tau_{\text{ref}}). \tag{7}$$

where $X_1(t - n\tau_{\text{ref}})$ is the phase term of the beat signal from the auxiliary interferometer with the time delay of $t - n\tau_{\text{ref}}$. $X_1(t - n\tau_{ref})$ can be derived from the beat signal through the Hilbert transformation. Therefore, the phase term $X_N(t)$ of the beat signal at the time $N\tau_{\text{ref}}$ can be calculated based on (7). And the phase term between at the time between every $N\tau_{ref}$ can be calculated using interpolation. The time at every increment of $X_N(t)$ is marked. And the signal from the main interferometer is then re-sampled at the marked time for the following demodulation similar as the frequency sampled data. With this method, the measurement length was extended to 40 km, which far beyond the coherence length. But the signal processing became complicated with a process time around 10 min.

Ding *et al.* used a deskew filter method for OFDR nonlinear phase noise compensation [14], [20], [45], which is firstly used in frequency modulated continuous wave (FMCW) Synthetic Aperture Radar (SAR) as a nonlinear frequency chirp solution [46], [47]. The system with the configuration shown in Fig. 8 has a main interferometer with an auxiliary interferometer. The nonlinear phase noise was considered as a factor multiplied on the signal from the main interferometer. As shown in Fig. 9, the phase noise can be estimated from the auxiliary interferometer signal using Hilbert transform, and can be compensated utilizing a deskew filter method. With this method, the spatial resolution of the OFDR system was 80 cm over 80 km FUT, which was around 187 times higher than the standard OFDR system.

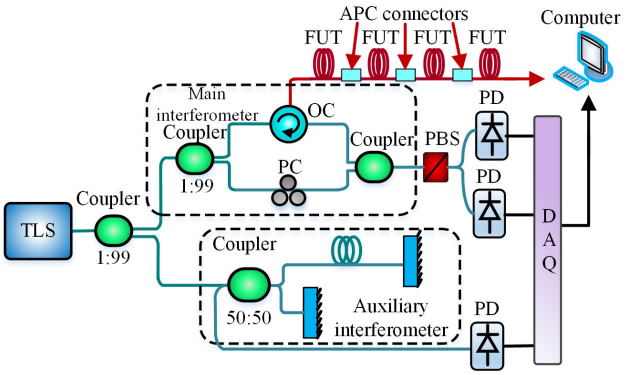


**FIGURE 8.** Configuration of OFDR system using deskew filter method.

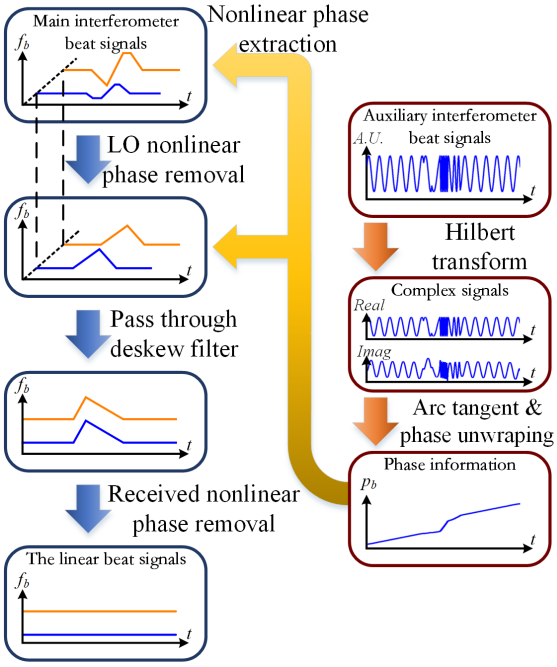


**FIGURE 9.** Signal processing procedure of deskew filter.

### 3) SHORT TUNING RANGE BASED METHOD

The linearity of the frequency sweep is deteriorated with the increase of the sweep period, which results in an aggravating of the phase noise. So, the phase noise can be mitigated by decreasing the frequency tuning period through decreasing the tuning range or increasing the tuning rate. The short tuning period increases the sweep linearity and furthermore increases the sensing range. But it restricts the spatial resolution of the OFDR system to several tens of meters as a disadvantage [48].

Geng *et al.* presented an OFDR system with a TLS whose tuning range was 380 MHz and achieved a sensing range of 95 km [49]. Arbel *et al.* utilized a TLS with a tuning rate of ∼1012 Hz/s to reduce the tuning period to 16 $\mu$s, and achieved a dynamic OFDR system for distributed acoustic

sensing [48]. The system can sense acoustic signals along a 10 km FUT.

#### 4) OTHER PHASE NOISE COMPENSATION METHODS

Ding *et al.* presented an OFDR system with a sensing range beyond the laser coherence length [50]. The system configuration consists of the main interferometer of the conventional OFDR systems. Besides the analysis of the backscattered signals from OFDR system, the phase noise term was also analyzed to deduce the position and intensity of the refection. The system can sense the Fresnel reflection in a distance of up to 170 km and the Rayleigh backscattering in a distance of up to 120 km using a TLS with only 13.6 km coherence length.

Shiloh *et al.* used a Fractional Fourier Transform (FrFT) instead of the conventional FFT to analyze the signals from a conventional OFDR system with a main interferometer [51]. The system has a 2.8 m spatial resolution on 20 km FUT.

Baker *et al.* used a Kerr phase-interrogator to analyze the signals from the OFDR system and achieved an incoherent OFDR system [52]. The system analyzes the Fresnel reflection of the FUT instead of the Rayleigh backscattering. The spatial resolution is around 11.2 cm at 151 km.

Liu *et al.* presented a modified OFDR system named time-gated digital OFDR (TGD-OFDR) to solve the phase noise caused by the nonlinear phase issue [53]. The system had the configuration shown in Fig. 10. The frequency-stable continuous light from the laser source was split into two beams into the measurement arm and the reference arm, respectively. The measurement light in the measurement arm was frequency-swept and time-gated by an AOM, while the reference light in the reference arm kept frequency-stable. The Rayleigh backscattering light and the reference light were beating and sampled. In order to retrieve and divide backscattering signals from different points of the FUT through data processing, the beating results were then multiplied with an equivalent reference signal, which had the similar frequency-sweep rate as the measurement light. Signals in different time and frequency in the multiplied results are signals from different points of the FUT. The time-gated measurement light had a narrow time window, which resulted in an easily achievement of high frequency-sweeping linearity and low nonlinear phase noise. The TGD-OFDR system has a 1.6 m spatial resolution over 110 km long fiber link. In addition, TGD-OFDR system was upgraded by adding a phase extraction module [54]. The FUT backscattering signal and the local reference signal are mixed in a 90-degree optical hybrid before collected by the photodiode for phase extraction. The modified system has a spatial resolution of 3.5 m with a 40 km measurement range.

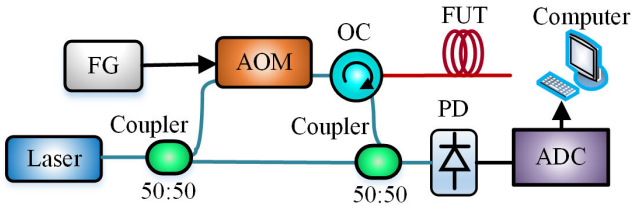


**FIGURE 10.** Configuration of TGD-OFDR system.

A brief list of the OFDR system based on different kinds of phase noise compensation methods with their performance summary is shown in Table 3.

**TABLE 3.** Performance summary of phase noise compensation methods based OFDR system.

| Type | Method | Sensing Range | Spatial Resolution |
|---|---|---|---|
| Frequency-sampling method | Frequency-sampling trigger [36] | 35m | 50um |
| | Frequency-multiplied trigger [38] | 4.48km | 100um |
| Software algorithms | NUFFT[36] | 50m | 5cm |
| | CGP [55] | 40km | 6cm |
| | Deskew filter[45] | 80km | 80cm |
| Short Tuning Range Based Method | vibrational and acoustical sensing[48] | 10km | Dozens of meters |
| | FMCW[49] | 95km | Not mentioned |
| Other Phase Noise Compensation Methods | Sensing range beyond the laser coherence length[50] | Rayleigh 120km | 200m |
| | FrFT instead of the conventional FFT[51] | 20km | 2.8m |
| | Phase-interrogator to analyze[52] | 151km | 11.2cm |
| | TGD-OFDR[53] | 110km | 1.6m |
| | Upgraded TGD-OFDR by adding a phase extraction module[54] | 40km | 3.5m |

### C. POLARIZATION-INDUCED FADING SOLUTIONS IN OFDR SYSTEM

In OFDR system, birefringence occurs in the single mode fiber (SMF) as the FUT, which causes the fluctuation of the backscattered light signal polarization state. The result is the fluctuation of the beating signal amplitude, which makes it hard to identify the local RBS spectral shift accurately. The effect is the polarization-induced fading (PIF), which has a severely impact on the measurement accuracy of the OFDR system and many other optical sensing systems using optical heterodyne detection technique.

In order to solve the polarization-induced fading issue, comes the polarization diversity detection (PDD). Soller *et al.* used PDD in OFDR to track the traverse light polarization state changes of the light as it traverses the birefringent light medium [37]. The modified system with the configuration shown in Fig. 11 used a polarization beam splitter (PBS)

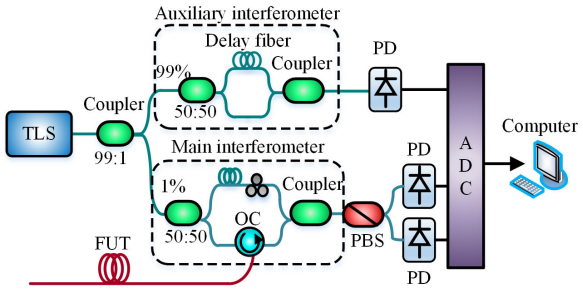


**FIGURE 11.** Configuration of OFDR system with PDD method for PIF solution.

to divide the measurement and reference signals into two mutually orthogonal polarization states, S and P. The measurement and reference signals of the same polarization state are combined. Beating and collected in the following analog to digital converter (ADC) and the results of the beating are analyzed in the computer for polarization state demodulation. Ding *et al.* utilized PDD in a conventional OFDR system as the solution to PIF [56]. The system shares the similar configuration as [37], and also used a polarization maintain coupler for recombination of the reference and measurement light signals. The beating results of the S and P polarization states are analyzed for PIF solving. The system with PDD scheme successfully eliminated the PIF and achieved a high accurate strain measurement in a 50 m standard SMF.

### *D. SIGNAL PROCESSING METHOD IN OFDR SYSTEM*

In OFDR system, strain or temperature variation on FUT causes a position change of the local spatial domain spectrum, and the strain or temperature change is proportional to the local spectrum position change value. Thus, calculating the location change of the spectrum by analysis of the measurement and reference signals is the approach to demodulate strain or temperature. The conventional demodulation procedure in OFDR system, which is mentioned in section II, is based on cross-correlation between backscattering signal and reference signal. The procedure works efficiently in sensing scenarios with short range, light strain or temperature change. Nevertheless, the performance diminished in other conditions. And the efficiency of conventional demodulation process decreases considerably with the increase of sensing range and spatial resolution requirement. Several methods have been put forward for signal processing and demodulation modification, to fit the system into more strict sensing conditions and improve the effectivity of the demodulation.

#### 1) SENSING RANGE AND SPATIAL RESOLUTION IMPROVEMENT

One of the main drawbacks of conventional OFDR system is the sensing range, which is limited by several factors such as coherence length and frequency tuning span. The sensing range restricts the usage of OFDR system. For fitting into more sensing conditions, Yin *et al.* presented a novel modified demodulation method for conventional OFDR shape sensing system, which used local spectrum matching, in order to eliminate the fake peaks and multi-peaks in the result of demodulation [57]. The configuration shown in Fig. 12 utilized an auxiliary interferometer to compensate the phase noise and the PDD to solve the PIF. Instead of performing cross-correlation, the presented method performed a local spectrum matching between each pair of time-domain measurement and reference signals. The signal processing procedure of local spectrum matching is as follows:

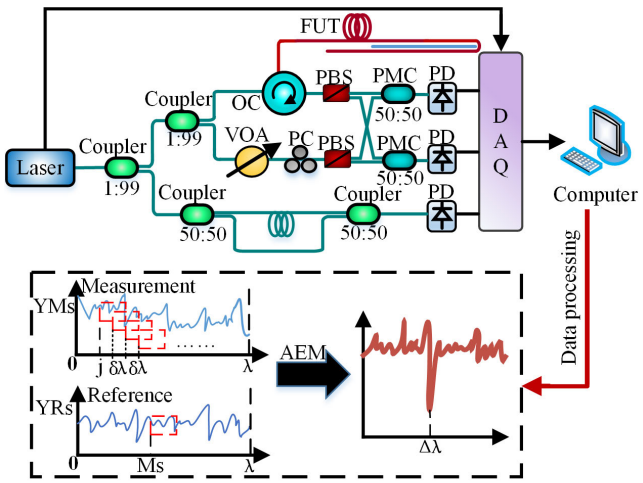


**FIGURE 12.** (a) Configuration of OFDR system using local spectrum matching demodulation method. (b) Signal processing procedure of spectrum matching demodulation method.

*Step 1:* In each pair of time-domain local measurement and reference signals, extracting a given section of reference signal within the entire reference spectrum and defining the signal section as the local reference spectrum.

*Step 2:* In the similar pair of time-domain local measurement and reference signals as step (1), applying a moving window to the local measurement signal to extract a series of local measurement spectrums. Matching the local reference spectrum from step (1) with each one of the local measurement spectrums.

*Step 3:* Moving the window applied to the local measurement signal to extract different measurement spectrums. Comparing the similarity between the local reference and each one of measurement spectrums by calculating the average Euclidean metric (AEM) between the local reference and measurement spectrum, and finding out the minimum AEM value which represents the highest similarity.

*Step 4:* The local wavelength shift is linearly determined by the window index with the minimum AEM as follows:

$$\Delta\lambda = (j_{\min} - M_s)\delta\lambda \tag{8}$$

where $\Delta\lambda$is the local wavelength shift, $j_{min}$ is the index of the window with the minimum AEM, $M_s$ is the wavelength sample interval.

Using local spectrum matching method, the system has a spatial resolution of 9.5 mm along 1 m sensing fiber with a shape reconstruction error less than 1 cm.

Besides, Cui *et al.* utilized a spectrum registration method to replace the conventional cross-correlation method in OFDR demodulation for dynamic OFDR strain sensing [58]. The spectrum registration method also uses the method which extracts local measurement and reference spectrum by sliding windows, and compares the similarity between them to locate the window index of the best spectrum similarity. The comparison between local spectrums is accomplished by calculating the similarity comparison index between them. Through spectrum registration method, the data volume to be compute is diminished in comparison to conventional cross-correlation approach, which simplifies the demodulation process and increases the measurement rate up to 800 Hz. In large strain or temperature variation scenarios, the variation causes an obvious location shift of the local backscatter spectrum. And the location shift accumulates along the FUT, which results in an increasingly obvious deviation. The result is that the local reference and measurement signal intervals, which are divided by sliding windows on the same position of the backscatter spectrum, mismatch with each other and the conditions of the same physical FUT segment are not compared due to the location shift. Cui *et al.* also presented a spatial calibration method for static OFDR strain sensing where large strain variation occurs. The method shares the similar principle with the spectrum registration method. The OFDR system with this method achieved an accurate demodulation of a strain larger than 7000 $\mu\varepsilon$. In addition to spectrum registration as the location-deviation compensation algorithm, Luo *et al.* calculated the deviation using the thermal/elastic-optic coefficients and rebuilt the Rayleigh backscatter spectrum from the calculated deviation [59]. The OFDR system based on this location-deviation compensation algorithm achieved a 0.5 mm spatial resolution with strain measurement accuracy of $\pm 15\mu\varepsilon$ at the end of a 25 m FUT.

In a conventional OFDR system, the sensing range is restricted by the frequency sweep period for a given sweep range, because backscatter signals from different sweep periods cannot be discriminate, which causes range ambiguity problem. This problem makes a tradeoff between sensing range and spatial resolution, as for a given sweep range, a higher sweep repetition rate comes to a better spatial resolution, however decreases the sweep period, which results in a shorter sensing range. In order to solve the issue, Nicolas *et al.* proposed digital interferometry OFDR (DI-OFDR) system [60], [61]. The system setup shown in Fig. 13 add an EOM in the measurement arm of the main interferometer for measurement light modulation. The measurement light signal is phase modulated by an EOM using a time-varying pseudorandom noise (PRN) code. The modulation process time stamps the signal. The beating signal of the reference light and the backscattering light is decoded with the matched PRN code. With this method, measurement signals in different sweep periods can be distinguished by

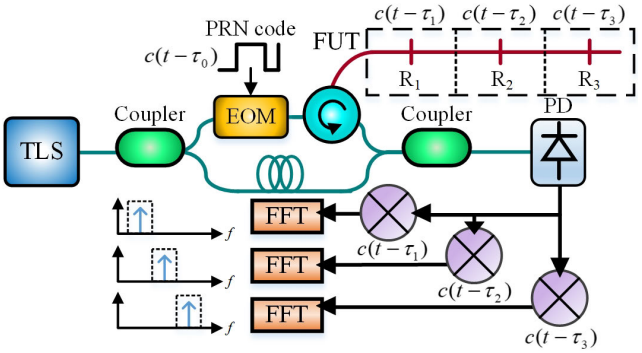


**FIGURE 13.** Setup and signal processing procedure of DI-OFDR system.

different time stamps and the range ambiguity of OFDR system is overcome. The procedure allows high repetition rate, short period frequency sweep without deterioration of sensing range, which shows promise in scenarios in need for both sensing range and spatial resolution.

In conventional OFDR signal processing, the conjugate term from the conventional FFT procedure results in a symmetrical frequency spectrum, with half of the transformed data from the sampled signal and the other half of data mirrored with the transformed one. This issue, which is referred to as positional ambiguity, causes only half of the frequency spectrum available, which reduces the measurement range of conventional OFDR into half of the coherence length of the laser source. Kim *et al.* modified the conventional OFDR system with a technique stem from bidirectional determination [62], [63]. The system setup is shown in Fig. 14. The length of the reference arm of the main interferometer was set to half of the FUT for (+) and (−) directions scattered light acquisition. And a $3*3$ coupler interferometry was combined with differential photo detectors for a phase-shifting signal acquisition. The acquired signals were formed to a complex signal. The FFT result of the complex signal was a frequency spectrum which overcame the positional ambiguity, with the whole spectrum available for analysis. With this method,

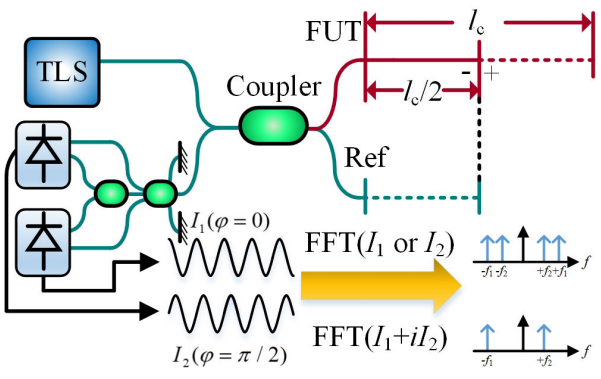


**FIGURE 14.** Configuration of OFDR system with bidirectional determination.

the sensing range of OFDR system was increased twofold without spatial resolution deterioration.

The spectrum analysis in conventional OFDR system requires division of the spatial domain signals with sliding window. A trade off problem occurs between measurement accuracy and spatial resolution as increasing the sliding window causes an improvement of the accuracy while worsen the spatial resolution and vice versa. Thus, the sliding window length needs to be set for maintaining a balance between sensing accuracy and spatial resolution. Wu *et al.* presented a theoretical model to estimate the OFDR measurement error and an algorithm to set the window length according to the measurement error [64]. The theoretical model estimates the measurement error based on the noise and a defined quality factor of the sampled signal. The algorithm can determine the sliding window length more reasonably, which maintain a balance between sensing accuracy and spatial resolution. Ding *et al.* utilized interpolation technique in the spectrum analysis process of OFDR system to solve the problem [65]. Each spatial domain local signal interval, which is divided by the spatial sliding window, is interpolated by padding zeros at one end of the data before inverse FFT. In this way, each signal interval has more points of data for spectrum analysis, thus causing an enhancement of the measurement resolution and accuracy without enlarging the length of the sliding window and deteriorate the spatial resolution. The OFDR system using interpolation shows the capacity of distinguishing 3 $\mu\varepsilon$ within 1 cm with uncertainty of 3.3 $\mu\varepsilon$ at a distance of 21.4 m. Besides, Feng *et al.* replaced the conventional STFT with Morlet wavelet transformation to reduce the tradeoff between sensing accuracy and spatial resolution [66]. The wavelet analysis can be regarded as the time-frequency analysis of the time domain signals. Due to the analysis method, the length of the sliding window of wavelet analysis varies along with its position in the spatial spectrum. Better spatial resolution can be achieved within short distance. The OFDR system with wavelet analysis process has a spatial resolution of 5 mm and a sensing accuracy better than 1 $\mu\varepsilon$.

Cui *et al.* combined the 2D image processing with the demodulation process of the OFDR system to denoise the signal [67]. The cross-correlation results between the local reference and measurement signals from each location of FUT are gathered to build a 2D image which contains the cross-correlation values and location. The 2D image is then processed through several image denoising methods including mean value filter, non-local means filter, and wavelet denoising method. The strain can be deduced from the denoised image with 1/5 to 1/10 measurement standard deviation within 3 mm sensing range. The system with 2D image denoise process shows promise in high accuracy distributed strain sensing in extreme short sensing range.

### 2) MEASUREMENT EFFICIENCY IMPROVEMENT

The conventional demodulation process of OFDR system is based on FFT for time-frequency conversion and cross-correlation for local Rayleigh frequency shift extraction. However, the processing efficiency of conventional FFT and cross-correlation diminish obviously with the increase of the data amount, which limit the velocity of OFDR sensing. For effectivity improvement, Park *et al.* proposed a real-time OFDR system based on real-time Fourier transformation (OFDR-RTFT) [68]. Utilizing a designed optical frequency-to-time conversion based on pulse time stretching with a linearly chirped FBG (LCFG), the frequency domain feature of the interference signal can be derived directly from the time-domain signal in the proposed system, which boosts the demodulation process. The system achieved a real-time optical coherence tomography with sensitivities up to −61 dB.

Since frequency spectrum analysis is a crucial point in OFDR system, distributed Fourier transform becomes a key method for signal processing, which is time-consuming facing high accuracy sensing demand with large amount of data. Malacarne *et al.* proposed a new scheme referred to as real-time optical spectrum Fourier transformation (RT-OSFT), which directly calculate the Fourier transform of the signal in analog time domain [69]. The system with the setup shown in Fig. 15 add an RT-OSFT module to process the beating signal before sampled by PD. With this method, the need for ADC and digital signal post-processing are avoided, which enhances the signal processing speed. The scheme was utilized in an OFDR system for real-time demodulation and provided MHz level data update rates. Besides, Ma *et al.* replaced the conventional FFT algorithm with an approach referred to as FFT-segmented chirp-Z transform for a more efficient demodulation [70]. The approach combines conventional FFT and segment chirp-Z transform (SCZT), which is a more efficient algorithm for Fourier transform. The signal collected is firstly fast analyzed with a coarse FFT to locate the zoom bands with power value exceed a critical threshold, which need to be analyzed in more detail. The located zoom bands are analyzed using SCZT for detailed analysis. The SCZT process can be divided into several parallelized chirp-Z transform (CZT) processes and computed simultaneously. Thus, the signal processing speed is enhanced. The approach was implemented in an OFDR system and achieved 2 mm spatial resolution at a distance of 54 m with a processing time less than 2 s.

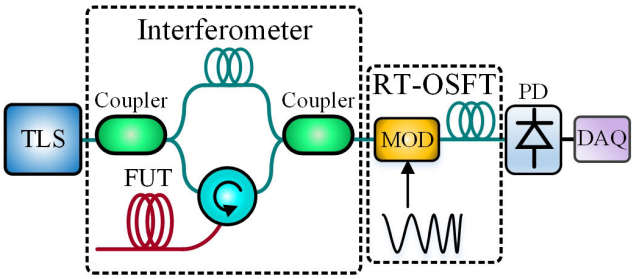


**FIGURE 15.** Configuration of OFDR system with RT-OSFT.

Wada *et al.* simplified the demodulation procedure of OFDR by regarding the wavelength shifts of the interfered

signals as the group delay [71]. The algorithm of calculating group delay of unstrained signals and strained signals was presented and proved to be more efficient than conventional signal processing based on STFT. Weighted averaging process was involved to solve noise problem. This method reduces the signal processing time into 3.5% of the conventional processing method based on STFT with high sensitivity.

Zhu *et al.* modified OFDR demodulation algorithm into activated weighted sliding windowed FFT [72]. The cross-correlation was calculated in a more efficient approach and the weighed sliding windowed FFT was used to acquire the Rayleigh backscatter involved frequency shifts. The modification improved the computational speed and memory use. In addition, a thresholding process based on the logistic activation function took place of the conventional thresholding function for noise cancellation. The proposed modulation process maintains a balance between measurement accuracy and demodulation speed.

A brief list of the OFDR system based on different kinds signal processing methods with their performance summary is shown in Table 4.

**TABLE 4. Performance summary of signal processing methods based OFDR system.**

| Method | Spatial Resolution | Sensing Range |
|---|---|---|
| Local spectrum matching[57] | 9.5 mm | 1 m |
| Spectrum registration[58] | 5 mm | N/A |
| Spectrum rebuild[59] | 0.5 mm | 25 m |
| DI-OFDR[60, 61] | 20 cm | 41 m |
| Bidirectional determination[62, 63] | 100 mm | 200 km |
| Spectrum interpolation[65] | 1 cm | 21.4 m |
| Wavelet transformation[66] | 5 mm | 8.7 m |
| 2D image processing[67] | < 3 mm | 50 m |
| Pulse time stretching[68] | 92.8 μm | 18 mm |
| RT-OSFT[69] | 34 μm | 9.4 mm |
| SCZT[70] | 2 mm | 54 m |
| Group delay calculation[71] | 1.03 mm | 50 mm |
| Activated weighted sliding windowed FFT[72] | 0.3 mm | 100 mm |

### E. OTHER ENHANCEMENTS IN OFDR SYSTEM

Due to the weak Rayleigh backscattering in conventional SMF, the SNR is deteriorated which reduce the measurement range, sensing accuracy and spatial resolution. On one hand, Koshikiya *et al.* solved the problem by reducing noise volume. The FUT and the interferometers of the OFDR system are insulated against acoustic perturbation using a soundproof box [73]. The insulation effectively eliminates the phase noise hails from acoustic perturbation and the system achieved a 40 km measurement range, which is close to the theoretical value. Nevertheless, the insulation limits the usage of the system in sensing scenarios which require the exposure of the FUT to the sensing object. On the other hand, Bergman *et al.* solved the SNR problem by increasing the signal amplitude utilizing an amplifying module [74]. The module with the configuration in Fig. 16 was added between the OFDR interrogator output and the FUT. The system with the amplifying module acquired an improvement of the one-way tolerable loss by 5 dB.

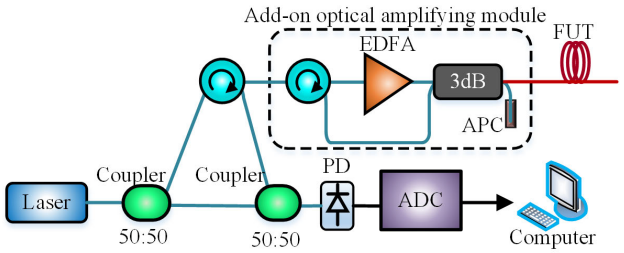


**FIGURE 16. Configuration of OFDR system with an add-on optical amplifying module.**

Gabai *et al.* proposed an OFDR system with I/Q detection [75]. The I/Q beating signal components are acquired using a coherent optical-communication-type receiver, and are combined to a complex signal with an asymmetric frequency spectrum. With this signal processing method, the modified system makes use of both the positive and negative beat frequencies to enhance the effective measurement range.

## IV. OFDR-BASED DISTRIBUTED OPTICAL FIBER SENSING

As is mentioned in Section II, the RBS shifts of the FUT segments are associated to the local temperature and strain changes. By analyzing the RBS shifts of the FUT, distributed temperature and strain sensing can be achieved. Besides, several other sensing parameters can be converted into changes of temperature or strain by particular system configurations. Therefore, OFDR-based distributed optical fiber sensing systems can be used under scenarios more than temperature and strain sensing. In this section, we mainly reviewed the basic applications including strain and temperature sensing of OFDR system. We would also mention other applications of OFDR systems including sensing of vibration, transversal pressure, 3D shape, magnetic field, refractive index, radiation, gas, and flow rate.

### A. TEMPERATURE AND STRAIN SENSING

#### 1) TEMPERATURE AND STRAIN DEMODULATION

Froggatt *et al.* presented an OFDR-based distributed fiber strain or temperature sensing method which is mentioned in section II.B and II.C [13], [16]. The system utilizes standard single-mode or gradient index multimode fiber and has millimeter-range spatial resolution over tens of meters of FUT, with strain and temperature resolution over 1 $\mu\varepsilon$ and 1 °C.

Zhou *et al.* presented time-resolved OFDR for a dynamic strain sensing, and achieved 10 cm spatial resolution of 17 m sensing length [76].

Sang *et al.* presented an OFDR-based temperature sensing method using gold coating SMF [77]. The technique provides

temperature sensing from 25 to 850 °C with 1 cm spatial resolution over an 1 m fiber segment. It shows promise in temperature sensing in harsh environments with high accuracy and stability.

Boyd *et al.* utilized OFDR-based sensing system for the superconducting degaussing cables temperature sensing under temperature down to 5 K [78], [79]. The high sensitivity of OFDR temperature sensing system compensated for low thermal sensitivity in optical fiber under low temperature scenario. They achieved temperature monitoring under temperature from 300 K to 5 K with 7 mm spatial resolution on 2 m SMF. They further extended the sensing range up to 20 m with cryogen monitoring abilities down to 15 K.

LUNA Tech Inc. (Roanoke, VA, USA) has developed OBR 4600, a commercial OFDR product for fiber distributed sensing. The system has a ±1.0 cm spatial resolution over 30 m or 70 m, with strain resolution up to ±1.0 $\mu\varepsilon$. The sensing range can also be extended to 2000 m in extended range mode. They have also developed ODiSI-B 5.0 for dynamic strain sensing, and achieved 5.2 mm spatial resolution of 2 m sensing length, with strain sensing accuracy up to ±15 $\mu\varepsilon$.

### 2) TEMPERATURE AND STRAIN DISCRIMINATION

The OFDR-based sensing system can measure temperature and strain simultaneously. And that leads to the issue of cross-sensitivity between temperature and strain. RBS shifts caused by temperature changes can influence strain sensing and vice versa. So, the discrimination between temperature and strain is an essential issue for the high precision OFDR-based sensing.

Froggatt *et al* [80], Froggatt [81], and Li *et al* [82] presented the discrimination method utilizing polarization maintaining fiber (PMF). The OFDR system configuration using PMF as the FUT is shown in Fig. 17. The discrimination is performed by autocorrelation and cross-correlation of the reference signal and the measurement signal. For reference signal and measurement signal of each spatial segment of the FUT, an autocorrelation is performed. For each pair of reference signal and measurement signal of the same segment, a cross correlation is performed between them. The differences between the peak shift of autocorrelation results of reference signal and that of measurement signal are calculated. The peak shift of cross-correlation results is also calculated. Both results are linear related to temperature and strain but with different coefficients. The temperature and strain discrimination can be achieved by calculating a parameter matrix of the temperature/strain coefficients.

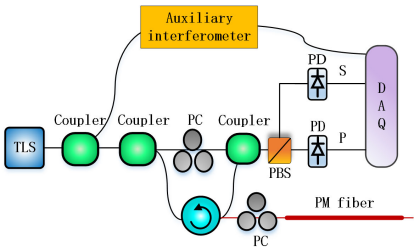


**FIGURE 17.** Configuration of OFDR system for simultaneous distributed strain and temperature measurement using PM fiber.

Zhou *et al.* presented a discrimination method between temperature and strain by using OFDR system and BOTDA system to the same FUT [83]. The method with system configuration shown in Fig. 18 combines the two systems together utilizing 1310/1550 nm wavelength division multiplexers (WDM), with OFDR system running in the wavelength of 1550 nm and B-OTDA system running in the wavelength of 1310 nm. The two systems are operated one immediately after another. The acquired Brillouin frequency shift (BFS) and RBS are both linear related to temperature and strain with different coefficients. And the temperature and strain discrimination can be achieved by calculating a parameter matrix of the temperature/strain coefficients of the RBS shifts and the BFS shifts. The system has a spatial resolution of 50 cm on 92 m fiber, with the temperature and strain measurement accuracy of ±1.2 °C and ±15 $\mu\varepsilon$.

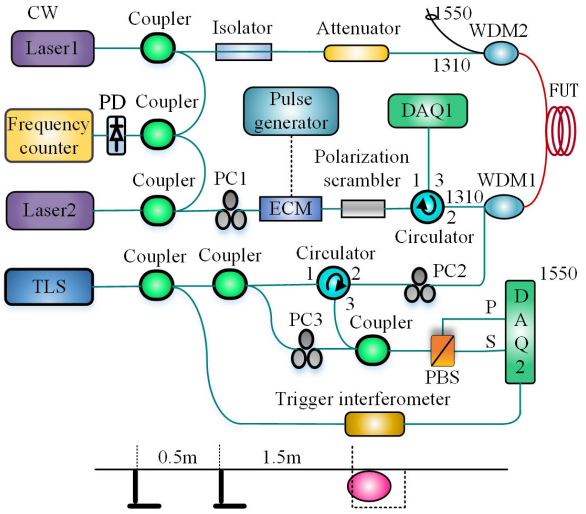


**FIGURE 18.** Configuration of the strain and temperature measurement system with OFDR and B-OTDA.

Ding *et al.* presented a discrimination method between temperature and strain using two OFDR-based sensing with two different kinds of SMF as the FUT [84]. The method with the system configuration shown in Fig. 19 utilizes two OFDR systems with different kinds of FUT. One is the standard SMF while the other is the reduced-cladding SMF (RC SMF). The two types of FUT are paired side by side as the sensing fiber in order to measure the same sensing parameters. As the RC SMF and the standard SMF have different sensitivity responses to temperature and strain, the RBS shifts of two OFDR-based systems are both linear related to temperature and strain variation but with different coefficient. The temperature and strain discrimination can be performed by calculating a parameter matrix of the temperature/strain coefficients of two RBS shifts. The system has a spatial resolution of

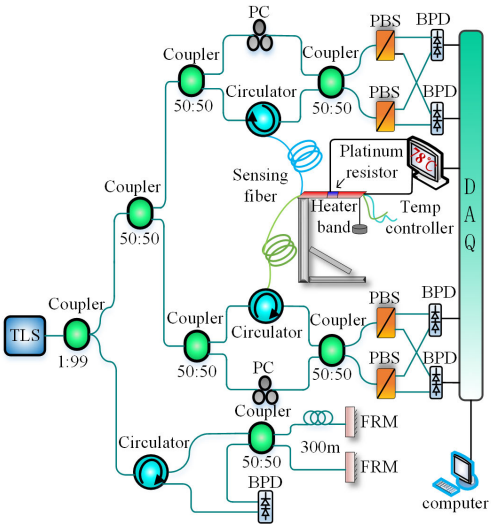


**FIGURE 19.** Configuration of the strain and temperature measurement system with 2 separated OFDR systems using different SMFs.

18 cm on 50 m range, with ±0.31 °C and ±7.97 $\mu\varepsilon$ measure accuracy.

#### 3) FBG-BASED OFDR TEMPERATURE AND STRAIN SENSING

By replacing the sensing fiber with FBG-embedded fiber of the conventional OFDR system, OFDR system with the setup shown in Fig. 20 is capable of FBG-based OFDR temperature and strain sensing. Eum *et al.* utilized long-gage FBGs with 10 mm length in conventional OFDR system for manufacturing process and strain monitoring of a composite structure made by vacuum-assisted resin transfer molding (VaRTM). The system measures temperature of the resin and preform during resin flow process in VaRTM, and measures the strain distribution during bending test. The system realizes a spatial resolution of around 1 mm. Besides, Murayama utilized 100 mm long-length FBGs in the conventional OFDR system for single-lap joint strain monitoring. Ning *et al.* studied the dynamic strain distribution measurement of an adhesive-bonded single-lap joint through a cyclic load test with FBG-based OFDR system. By analysis of the strain distribution measurement data, the crack detection method was performed as well. Wada *et al.* presented a dynamic strain monitoring technique utilizing FBG-based OFDR, which was used for helicopter blade vibration monitoring. The system used a 5 m FBG bonded to a 5.5 m helicopter blade model, and achieved a sensing spatial resolution of 1 mm within 20 m sensing range. Li *et al.* developed a dense ultra-short (DUS)-FBG array, and used the FBG array in OFDR system for distributed strain and temperature sensing with high spatial resolution. Every FBGs of the DUS-FBG array shares the length of 1 mm. And the space between each adjacent FBGs is 500 $\mu$m. The 10 m long sensing fiber contains 6680 FBGs. The system achieved a 1.00 °C temperature precision and 20.02 $\mu\varepsilon$ strain precision.

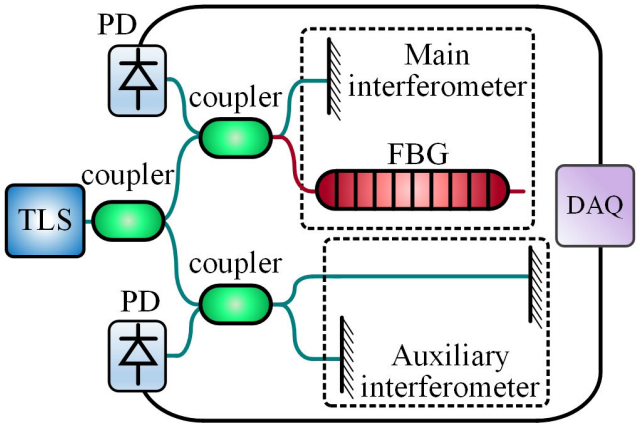


**FIGURE 20.** Experimental setup of FBG-based OFDR system.

### B. VIBRATION SENSING

The OFDR system can also realize distributed vibration sensing along the FUT. Ding *et al.* presented a cross-correlation similarity analysis (CCSA) method utilizing standard OFDR system [85]. This method analyzes the spatial domain reference and measurement signals, which are the FFT results of the reference and measurement beating signals, to sense the vibration. The measurement and signal processing procedure shown in Fig. 21 is mostly similar to the procedure of the OFDR signal demodulation, which is mentioned in section 2.2.

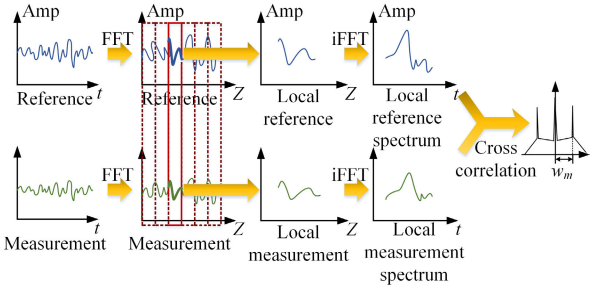


**FIGURE 21.** Demodulation procedure of OFDR system for vibration position and frequency measurement.

The result of the cross-correlation has different attribute related to the vibration state. As is shown in Fig. 22. When there is no local vibration, the cross-correlation result has one center peak with high amplitude. Whereas, when a local vibration occurs, the cross-correlation result has multiple disordered peaks with low amplitude. To quantitatively analyze the result, a "non-similar level" is defined to estimate the amount and intensity of the peaks. The non-similar level is the number of data points that beyond the threshold value in the cross-correlation result. The threshold is a certain ratio of the highest cross-correlation peak. The non-similar level represents the intensity of the local vibration. By demodulating the non-similar levels along the FUT, the OFDR-based

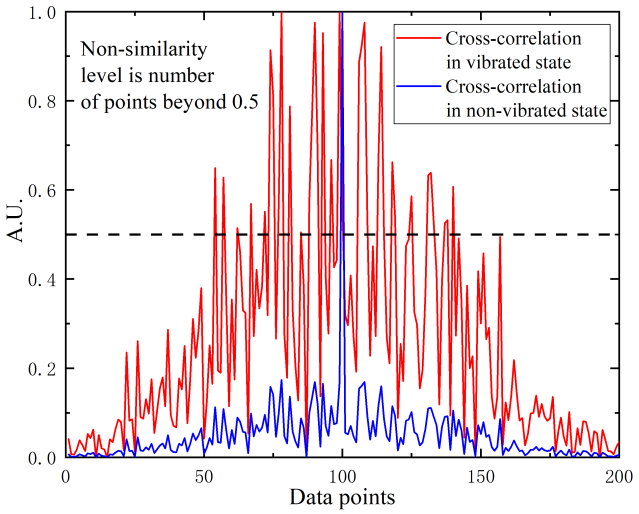


**FIGURE 22.** Cross-correlation spectrums between local rayleigh backscattering in vibrated and non-vibrated states for vibration measurement.

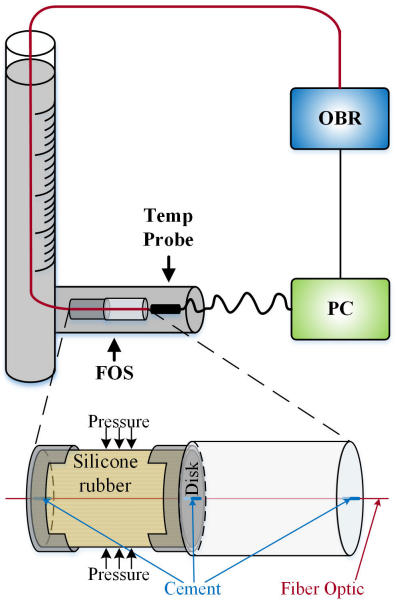


**FIGURE 23.** Experimental setup of transversal pressure sensing OFDR system.

system achieved a distributed vibration sensing with a spatial resolution of 5 m on a standard 12 km SMF.

Based on the CCSA method, Ding *et al.* utilized an optical deskew filter method for the phase noise compensation in OFDR system, and extended the vibration sensing range to 40 km with a spatial resolution of 11.6 m [86]. By adding spectral shift and "V" shape as two alternative signal characteristics other than non-similarity level, the vibration sensing range is extended to 92 km with a spatial resolution of 13 m [87].

Wang *et al.* presented a distributed vibration sensing based on TGD-OFDR and phase-sensitive OFDR [54]. They used the standard TGD-OFDR system and measured multiple consecutive traces of the Rayleigh backscattering signal. The high tuning rate of TLS reduced the phase noise to a large extent. The vibration is observed by comparison of different signal traces. Vibration affects the length of the optical path, which causes the change of the backscattering signal phase. The phase variation is demodulated by comparison among different signal traces, and thus realized the measurement and localization of vibration. The system has a spatial resolution of 3.5 m on a 40 km measurement range. Steinberg *et al.* utilized the same principle for a dynamic high-sensitive distributed vibration sensing and achieved a sensing range of 101 km [88].

### C. TRANSVERSAL PRESSURE SENSING

Transversal pressure sensitivity of OFDR-based sensing systems is low, which makes direct sensing not feasible. Using polymers with high Poisson's ratio to linearly convert the transversal pressure into the longitudinal strain is the majority of the solutions. Schenato *et al.* presented a method utilizing silicone rubber to cover the FUT for OFDR-based transversal pressure sensing in riverbanks monitoring scenario [89]. The device shown in Fig. 23 consists of two chambers filled with silicone rubber, which is used for pressure and temperature sensing, respectively. The FUT of the OFDR system goes axially through the device. The system has temperature and pressure sensitivities of $-7$ GHz/°C and $-3.2$ GHz/kPa with accuracies of 0.5 °C and 0.3 kPa, respectively.

Besides using polymer-coated fiber to convert transversal pressure into longitudinal strain, the pressure can also be measured by sensing the birefringence in FUT. The transversal pressure along FUT causes local birefringence, which further result in a polarization state variation of the backscattering light. Therefore, by analyzing the backscattering light state of polarization (SOP), the local birefringence can be deduced, which reveals the local transversal pressure. Wei *et al.* presented a polarimetric optical frequency domain reflectometer (P-OFDR) for space-resolved transverse stresses sensing [90]. The system with the configuration shown in Fig. 24 is based on the principle mentioned above. The system utilizes 2 PBSs to divide the orthogonal polarized light signals of the interference light signals, which are detected by 2 PDs for analyze respectively to demodulate the local transversal pressure. The spatial resolution of the system is 0.5 mm with a fiber longer than 800 m.

### D. MAGNETIC FIELD SENSING

The polarization state of the backscattering light of P-OFDR system is affected by the magnetic field based on the Faraday rotation around the FUT. By analysis of the SOP of the backscattering light, OFDR-based system can demodulate the Faraday rotation along the FUT, and further sense the magnetic field. Palmieri *et al.* firstly utilized the P-OFDR system based on this principle to achieve a distributed sensing of electric current [91]. The system setup is shown in Fig. 25,

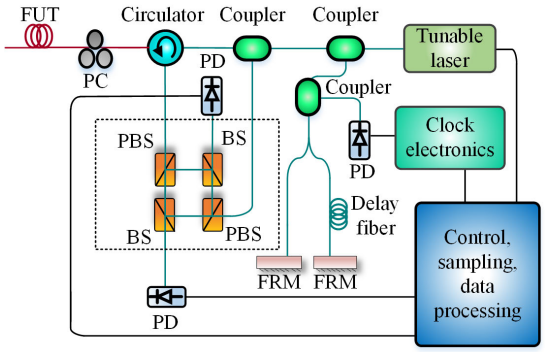


**FIGURE 24.** Configuration of transversal stress measurement system using P-OFDR.

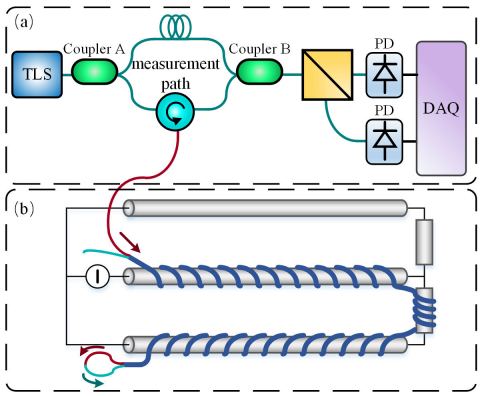


**FIGURE 25.** (a) Configuration of P-OFDR system. (b) Experimental layout for electric current measurement.

which uses a polarization controller to control the SOP of signal light. The FUT is helically wound around the conducting wire in order to sense the magnetic field along the wire, and further measure the electric current along the wire. The system achieved a spatial resolution of 4 m on a 400 m FUT.

The magnetic field can cause strain to magnetostrictive material based on magnetostriction. Du *et al.* presented an optical distributed magnetic field sensor based on the principle above [92]. The system with configuration shown in Fig. 26 utilizes magnetostrictive Fe-Co-V alloy thin films to convert magnetic field into strain. Part of the FUT is spliced and attached to the alloy films. The OFDR system measure the strain on FUT caused by magnetic field to demodulate the magnetic field around the FUT, with a spatial resolution of 4 cm in 51 m FUT.

### E. REFRACTIVE INDEX SENSING

Du *et al.* presented an OFDR-based refractive index (RI) sensing system utilizing macro-bending SMF as FUT [93]. They used the standard OFDR-based sensing system with part of the FUT bended. By bending part of the FUT to a certain radius of curvature, the RI of the external medium surrounding the bended fiber part would vary, thus causing local RBS shifts. The RI variation could then be demodulated

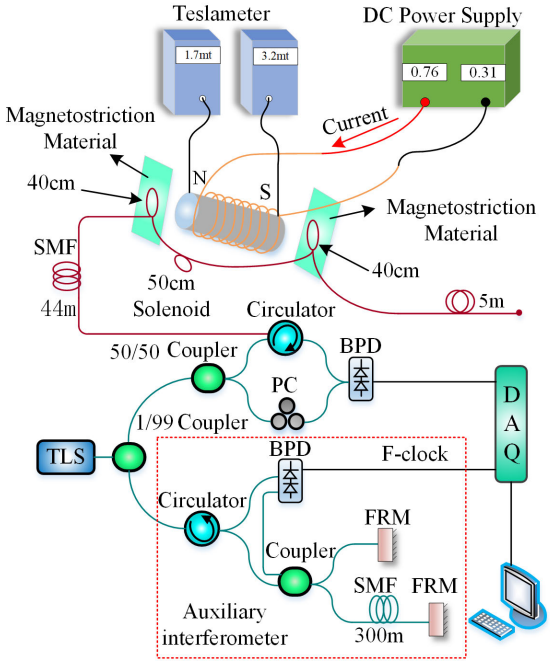


**FIGURE 26.** Configuration of OFDR system for distributed magnetic field measurement.

by analysis of the RBS. The system has a RI measurement sensitivity of 2319.2402 GHz/RIU (18.5502 nm/RIU) and 2717.8502 GHz/RIU (21.7402 nm/RIU) with bending diameters of 12.202 mm and 11.302 mm, respectively.

### F. RADIATION SENSING

Using radiation sensitive fiber as FUT allows the OFDR-based system to sense radiation. Faustov *et al.* presented a distributed radiation measurement system utilizing phosphor-silicate optical fiber as the radiation sensitive fiber [94]. The FUT of the system contains 3 sections as shown in Fig. 27. Sections 1 and 3 were standard telecommunication optical fiber, while section 2 was the phosphor-silicate radiation sensitive fiber. The principle of the measurement is based on the radiation induced absorption of the phosphor –silicate optical fiber. Section of the radiation sensitive fiber exposed to radiation would absorb the radiation, which causes the rise of the Rayleigh backscattering power. The OFDR system measure and compare the Rayleigh backscattering signal power before and after radiation. The radiation can be measured and located by the loss of the signal. The system realized a measurement range up to 100 kGy and a relative accuracy of around 20%, and can reconstruct the absorption dose distribution profile with a spatial resolution of 15 cm.

### G. GAS SENSING

Palladium (Pd) is a kind of material that can absorb hydrogen, which results in its extension. Using this material, the hydrogen amount can be converted into strain variation, which can be measured by OFDR-based system. Chen *et al.* presented

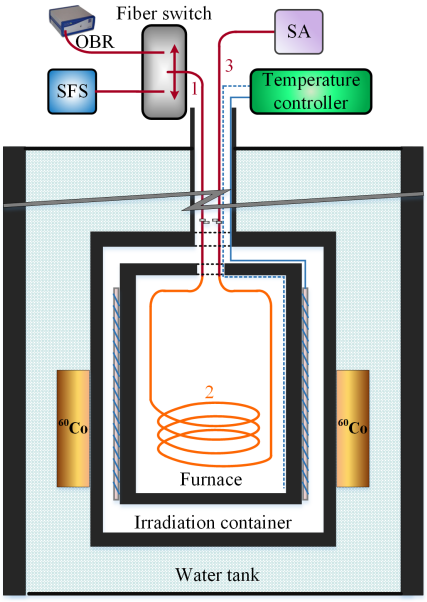


**FIGURE 27.** Experimental setup of OFDR system for radiation sensing.

an OFDR-based gas sensing system using the principle mentioned above for hydrogen measurement [95]. The system with the setup shown in Fig. 28 utilized a special fiber coated with copper (Cu) and Pd as FUT. Pd hydrogen absorption causes local strain variation which can be measured using OFDR system. The Cu coating can be heated by an electrical current, which increases the sensitivity of the system. The system achieved a distributed hydrogen sensing with a spatial resolution of 1 cm.

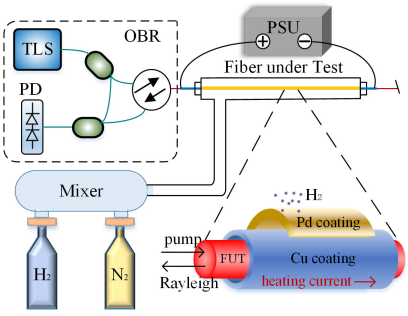


**FIGURE 28.** Experimental setup of OFDR system for distributed hydrogen sensing.

### H. GAS FLOW SENSING

Chen *et al.* presented an OFDR-based gas flow rate sensing system using self-heated optical fiber [96]. The system setup shown in Fig. 29 utilized Cu coated fiber as the FUT. The Cu coating can be heated by an electrical current, which causes the rise of local temperature to a certain point. And the gas flows blowing on certain location would cause the decrease of local temperature, which can be sensed by OFDR system. The system can detect the magnitude and location of the

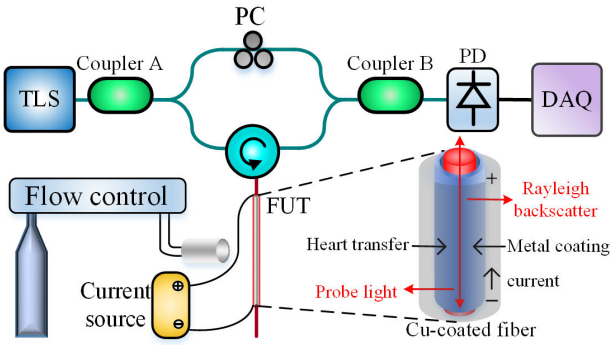


**FIGURE 29.** Experimental setup of OFDR system for gas flow sensing.

temperature variation, which is related to the local gas flow rate. The sensing spatial resolution is 1 cm. And with multiple paralleled fibers, the system can also sense the flow direction.

### I. 3D-SHAPE SENSING

3D shape sensing is a research hotspot which draws attention of a large number of researchers. The OFDR-based sensing system shows promise in 3D shape sensing because of its high sensing precision, ideal spatial resolution and elevated accuracy. Duncan *et al.* presented an OFDR-based 3d shape sensing system [97], [98]. The system with setup shown in Fig. 30 used 3 parallel fibers or 1 multi-core fiber as a sensing fiber triplet. The fiber triplet is divided into several segments. By fixing the beginning segment at a given reference point and using the data from the OFDR strain sensing of each segment, the locations and orientation of each segment can be deduced in turn. The 3D shape of the fiber triplet can be reconstructed by the location and orientation of each segment.

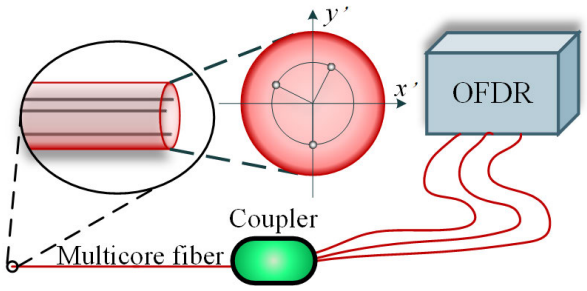


**FIGURE 30.** Experimental setup of OFDR system for 3D-shape sensing using multicore optical fiber.

Lally *et al.* utilized helical, multicore optical fiber as the sensing fiber in OFDR system for distributed shape sensing of flexible structures. The OFDR system with sensing fiber shown in Fig. 31 is capable of measuring distributed strain along the 3 cores. The data processing converts the distributed strain data from 3 cores into axial twist and curvature data along the sensing fiber, which can be then converted to 3D shape of the sensing fiber. The system achieved shape sensing with an accuracy of 0.4% – 1.3% by length over 20-30 m.

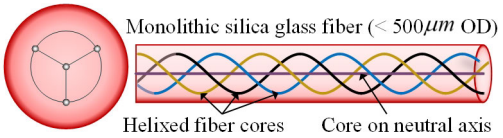


**FIGURE 31.** Helical multicore optical fiber for 3D-shape sensing.

Due to the high precision and real-time advantage, 3D shape sensing technique based on OFDR shows promise in biomedical domain applications. Parent *et al.* utilized the method for the guidance of minimally invasive medical instrument like surgical needle and catheters. By inserting 3 fibers inside the medical instrument, the strain data from 3 degrees can be obtained and the converted to 3D shape of the instrument. Using Rayleigh scattering enhanced fibers, the sensing precision was later enhanced [99]. The system achieved a near real-time medical instrument tracking, which showed promise in remotely controlled needle or catheter guidance. Parent *et al.* then utilized the OFDR 3D shape sensing system for shape and tip tracking of the catheter in intra-arterial liver cancer therapies. The shape tracking achieved an accuracy with 3D mean errors of 2.8±0.9 mm. Lorre *et al.* also utilized OFDR system for 3D shape sensing of biomedical instruments, and used 3 backscatter enhanced fibers to form a fiber triplet. The radial and angular positions of the 3 fibers in the triplet are measured for best measurement performance.

## V. SPECIAL-FIBER-BASED OFDR

### A. RAYLEIGH SCATTERING ENHANCED FIBER

The paramount limitation in the sensitivity and accuracy of OFDR sensing system hails from the low Rayleigh backscattering signal from the FUT. Loranger *et al.* presented a method to fabricate Rayleigh scattering enhanced fiber out of standard SMF [100]. The Rayleigh backscattering enhanced fiber is fabricated by a simple exposure of the standard SMF-28 fiber core to the continuous ultraviolet (UV) light, which increases the density of scattering defects. They perform the UV exposure using FBG writing system without writing an FBG. The high numerical aperture (HNA) fiber exposed to UV light shows the same improvement in Rayleigh signal. By using Rayleigh backscattering enhanced fiber as the FUT of OFDR system, the Rayleigh backscattering light can be enhanced by ten-fold, which therefore improves the SNR of the system. A 20 $m\kappa$ detection was achieved with 2 cm spatial resolution by utilizing the Rayleigh scattering enhanced fiber in the OFDR system. Besides, Yan *et al.* used femtosecond ultrafast laser radiation to fabricate Rayleigh scattering enhanced fiber with stable performance in extreme environments [101]. They utilized femtosecond ultrafast laser beam to scan the fiber core and realized more than 40 dB enhancement of Rayleigh backscattering signal. And the enhancement is stable from room temperature to 800 °C, which ensures a reliable temperature sensing in extreme environments. By using the Rayleigh scattering enhanced fiber in the OFDR system, a real-time monitoring of solid oxide fuel cell (SOFC) temperature with 5 mm spatial resolution was achieved at 800 °C in hydrogen gas environment. Although the optical loss (∼0.1 dB/cm) induced by ultrafast laser of the Rayleigh scattering enhanced fiber can be an essential drawback when used in distributed sensing with long interrogation lengths, it shows promise in harsh environment sensing with interrogation length less than 2 m.

### B. POLYMER OPTICAL FIBER

Polymer optical fibers (POFs) are another kind of feasible FUT for OFDR sensing system. Compared to standard silica-based optical fiber, POF has advantages in lower cost, better flexibility, and resistance to some kinds of physical and chemical attack factors. Kreger *et al.* firstly used POF as the FUT in the OFDR temperature and strain sensing system and indicated the feasibility of the usage [102]. The system has a strain and temperature resolution better than 4 $\mu\varepsilon$ and 1 °C at 70 m range. The sensitivity is roughly 20% higher than silica-based optical fiber with same sensing linearity and hysteresis. The results demonstrate that POF can be a promising alternative to silica-based fibers under scenarios where the advantages of POF are needed, such as shape sensing, RI sensing and so on.

### C. PHOTONICS CRYSTAL FIBER

Photonics crystal fibers (PCFs) or microstructured optical fibers (MOFs) have been used in OFDR systems under some special circumstances due to some special features. The radiation tolerance of MOF makes it an optional alternative for sensors in harsh environments such as nuclear power plants, space or high energy physics facilities [103]. In addition, PCF also shows promise in chemical sensing such as gas sensing [104].

## VI. CONCLUSION

We have made a thorough overview of the OFDR technology including sensing principles, performance enhancement and sensing applications. As a summary, we list some perspectives of the OFDR based sensing systems.

First, in terms of OFDR system performance enhancement, the software-based techniques are promising techniques for further development, including software-based phase noise compensation method, signal processing methods and other performance improvement based on software algorithm. The overarching drawback of the OFDR based sensing system is the nonlinear phase noise caused mainly by the nonlinear frequency tuning of the TLS. Besides the costly improvement of the TLS tuning linearity, several techniques for phase noise elimination and compensation have been presented and discussed, which can be classified into frequency-sampling method, software algorithms compensation method, and short-tuning-range-based method. The frequency-sampling method is simple for application but

has a limitation of sensing range by the length difference between the two arms of the auxiliary interferometer. The short-tuning-range-based method improves the linearity of the test light at the cost of the spatial resolution which limit the application in high accuracy measurement. The software algorithms compensation method takes tolls on the computation burden due to the increasing amount of data to process, which can be solved by using elevated performance computer or improvement of the algorithms. With the evolution of the computing power and the advance of some novel signal processing algorithms, the software-based algorithms compensation method shows promise in further performance enhancement of the OFDR system. Besides, improvements of the demodulation algorithms were also proposed, which also based on software-based signal processing.

Second, TLS plays an important part in the OFDR system performance. The narrower linewidth of the TLS can increase the sensing range of the OFDR system. The wide tuning range and high tuning linearity contribute to high spatial resolution and SNR. Furthermore, the high tuning rate can be critical in dynamic sensing. However, the linewidth, tuning range, tuning rate and tuning linearity face a trade-off with one increasement and others diminished. A TLS meets all the needs simultaneously can be costly, which restrain the application of the OFDR-based sensing system. Development of the high-performance TLS is one of the key aspects of the OFDR technology.

Lastly, OFDR-based technology shows promise in high-accuracy DOFS and can extend its application into broader sensing parameters. Due to the better sensing performance at a short range such as a higher spatial resolution and a shorter sensing period, OFDR becomes an ideal solution for high-accuracy DOFS like real-time 3D curve shape sensing and reconstruction, which can be widely used in construction industry, energy industry, automobile industry and aerospace industry. With its high spatial resolution and accuracy, OFDR can replace some FBG-based sensing in some scenarios. Furthermore, with usage of the special coating of standard SMF and special fibers as the sensing medium, the sensing parameters of OFDR can be extended into more than fiber imperfection, strain, and temperature. The OFDR system can sense chemical and biological parameters with certain configuration. And with the high sensing spatial resolution with high accuracy, OFDR technology has potential to meet sensing demands in some tough conditions.

## REFERENCES

[1] F. P. Kapron, D. B. Keck, and R. D. Maurer, "Radiation losses in glass optical waveguides," *Appl. Phys. Lett.*, vol. 17, no. 10, pp. 423–425, Nov. 1970.

[2] F. Kapron, R. Maurer, and M. Teter, "Theory of backscattering effects in waveguides," *Appl. Opt.*, vol. 11, no. 6, pp. 1352–1356, Jun. 1972.

[3] R. G. Smith, "Optical power handling capacity of low loss optical fibers as determined by stimulated Raman and Brillouin scattering," *Appl. Opt.*, vol. 11, no. 11, pp. 2489–2494, Nov. 1972.

[4] S. D. Personick, "Photon probe—An optical-fiber time-domain reflectometer," *Bell Syst. Tech. J.*, vol. 56, no. 3, pp. 355–366, Mar. 1977.

[5] Y. Wang, B. Jin, Y. Wang, D. Wang, X. Liu, and Q. Bai, "Real-time distributed vibration monitoring system using Φ -OTDR," *IEEE Sensors J.*, vol. 17, no. 5, pp. 1333–1341, Mar. 2017.

[6] X. Liu, B. Jin, Q. Bai, Y. Wang, D. Wang, and Y. Wang, "Distributed fiber-optic sensors for vibration detection," *Sensors*, vol. 16, no. 8, p. 1164, Jul. 2016.

[7] T. W. Whitbread, W. S. Wassef, P. M. Allen, and P. L. Chu, "Profile dependence and measurement of absolute Raman scattering cross-section in optical fibres," *Electron. Lett.*, vol. 25, no. 22, pp. 1502–1503, Oct. 1989.

[8] F. Farahi, C. N. Pannell, and D. A. Jackson, "Potential of stimulated Brillouin scattering as sensing mechanism for distributed temperature sensors," *Electron. Lett.*, vol. 25, no. 14, pp. 913–915, Jul. 1989.

[9] T. Horiguchi, T. Kurashima, and M. Tateda, "Tensile strain dependence of Brillouin frequency shift in silica optical fibers," *IEEE Photon. Technol. Lett.*, vol. 1, no. 5, pp. 107–108, May 1989.

[10] T. Kurashima, T. Horiguchi, and M. Tateda, "Distributed-temperature sensing using stimulated Brillouin scattering in optical silica fibers," *Opt. Lett.*, vol. 15, no. 18, pp. 1038–1040, Sep. 1990.

[11] K. Shimizu, T. Horiguchi, Y. Koyamada, and T. Kurashima, "Coherent self-heterodyne detection of spontaneously brillouin-scattered light waves in a single-mode fiber," *Opt. Lett.*, vol. 18, no. 3, p. 185, Feb. 1993.

[12] W. Eickhoff and R. Ulrich, "Optical frequency-domain reflectometry in single-mode fibers," *Appl. Phys. Lett.*, vol. 39, no. 9, pp. 693–695, 1981.

[13] M. E. Froggatt and J. Moore, "High-spatial-resolution distributed strain measurement in optical fiber with Rayleigh scatter," *Appl. Opt.*, vol. 37, no. 10, pp. 1735–1740, 1998.

[14] Z. Ding, X. S. Yao, T. Liu, Y. Du, K. Liu, J. Jiang, Z. Meng, and H. Chen, "Compensation of laser frequency tuning nonlinearity of a long range OFDR using deskew filter," *Opt. Exp.*, vol. 21, no. 3, pp. 3826–3834, Feb. 2013.

[15] Y. Du, T. Liu, Z. Ding, Q. Han, K. Liu, J. Jiang, Q. Chen, and B. Feng, "Cryogenic temperature measurement using Rayleigh backscattering spectra shift by OFDR," *IEEE Photon. Technol. Lett.*, vol. 26, no. 11, pp. 1150–1153, Jun. 2014.

[16] S. T. Kreger, D. K. Gifford, M. E. Froggatt, B. J. Soller, and M. S. Wolfe, "High resolution distributed strain or temperature measurements in single- and multi-mode fiber using swept-wavelength interferometry," in *Proc. Opt. Fiber Sensors*, 2006, pp. 1–4, doi: 10.1364/OFS.2006.ThE42.

[17] K. Yüksel, M. Wuilpart, and P. Mégret, "Analysis and suppression of nonlinear frequency modulation in an optical frequency-domain reflectometer," *Opt. Exp.*, vol. 17, no. 7, pp. 5845–5851, 2009.

[18] E. D. Moore and R. R. Mcleod, "Correction of sampling errors due to laser tuning rate fluctuations in swept-wavelength interferometry," *Opt. Exp.*, vol. 16, no. 17, pp. 13139–13149, 2008.

[19] X. Fan, Y. Koshikiya, and F. Ito, "Phase-noise-compensated optical frequency domain reflectometry with measurement range beyond laser coherence length realized using concatenative reference method," *Opt. Lett.*, vol. 32, no. 22, pp. 3227–3229, Dec. 2007.

[20] Y. Du, T. Liu, Z. Ding, B. Feng, X. Li, K. Liu, and J. Jiang, "Method for improving spatial resolution and amplitude by optimized deskew filter in long-range OFDR," *IEEE Photon. J.*, vol. 6, no. 5, pp. 1–11, Oct. 2014.

[21] C. Henry, "Theory of the phase noise and power spectrum of a single mode injection laser," *IEEE J. Quantum Electron.*, vol. 19, no. 9, pp. 1391–1397, Sep. 1983.

[22] N. Fujiwara, H. Ishii, H. Okamoto, Y. Kawaguchi, Y. Kondo, and H. Oohashi, "Suppression of thermal wavelength drift in super-structure grating distributed Bragg reflector (SSG-DBR) laser with thermal drift compensator," *IEEE J. Sel. Topics Quantum Electron.*, vol. 13, no. 5, pp. 1164–1169, Oct. 2007.

[23] O. Boukari, L. Hassine, H. Bouchriha, and M. Ketata, "Study of dynamic chirp in direct modulated DFB laser for C-OFDR application," *Opt. Commun.*, vol. 283, no. 10, pp. 2214–2223, May 2010.

[24] O. Boukari, L. Hassine, O. Latry, M. Ketata, and H. Bouchriha, "Characterization of the chirp in semiconductor laser under modulation," *Mater. Sci. Eng., C*, vol. 28, nos. 5–6, pp. 671–675, Jul. 2008.

[25] Z. Deng, Z. Liu, B. Li, and Z. Liu, "Precision improvement in frequency-scanning interferometry based on suppressing nonlinear optical frequency sweeping," *Opt. Rev.*, vol. 22, no. 5, pp. 724–730, Oct. 2015.

[26] A. Y. Tkachenko, I. A. Lobach, and S. I. Kablukov, "Coherent optical frequency-domain reflectometer based on a fibre laser with frequency self-scanning," *Quantum Electron.*, vol. 49, no. 12, pp. 1121–1126, Dec. 2019.

[27] B. Golubovic, B. E. Bouma, G. J. Tearney, and J. G. Fujimoto, "Optical frequency-domain reflectometry using rapid wavelength tuning of a Cr4+:forsterite laser," *Opt. Lett.*, vol. 22, no. 22, pp. 1704–1706, Nov. 1997.
[28] C. Ndiaye, T. Hara, and H. Ito, "Performance of a solid-state frequency-shifted feedback laser in optical ranging," *J. Eur. Opt. Soc., Rapid Publications*, vol. 4, Mar. 2009, Art. no. 09010, doi: 10.2971/jeos.2009.09010.
[29] K. Nakamura, T. Hara, M. Yoshida, T. Miyahara, and H. Ito, "Optical frequency domain ranging by a frequency-shifted feedback laser," *IEEE J. Quantum Electron.*, vol. 36, no. 3, pp. 305–316, Mar. 2000.
[30] P. Oberson, B. Huttner, O. Guinnard, L. Guinnard, G. Ribordy, and N. Gisin, "Optical frequency domain reflectometry with a narrow linewidth fiber laser," *IEEE Photon. Technol. Lett.*, vol. 12, no. 7, pp. 867–869, Jul. 2000.
[31] Z. He, T. Kazama, Y. Koshikiya, X. Fan, F. Ito, and K. Hotate, "High-reflectivity-resolution coherent optical frequency domain reflectometry using optical frequency comb source and tunable delay line," *Opt. Exp.*, vol. 19, no. 26, pp. 764–769, Dec. 2011.
[32] J. Li, J. Du, S. Wang, L. Li, L. Sun, X. Fan, Q. Liu, and Z. He, "Improving the spatial resolution of an OFDR based on recirculating frequency shifter," *IEEE Photon. J.*, vol. 7, no. 5, pp. 1–10, Oct. 2015.
[33] L. Sun, J. Du, L. Li, and Z. He, "High order SSB modulation and its application for advanced optical comb generation based on RFS," *Opt. Commun.*, vol. 354, pp. 380–385, Nov. 2015, doi: 10.1016/j.optcom.2015.06.013.
[34] M. Badar, H. Kobayashi, and K. Iwashita, "Spatial resolution improvement in OFDR using four wave mixing and DSB-SC modulation," *IEEE Photon. Technol. Lett.*, vol. 28, no. 15, pp. 1680–1683, Aug. 1, 2016.
[35] B. Wang, X. Fan, W. Shuai, J. Du, and Z. He, "Millimeter-resolution long-range OFDR using ultra-linearly 100 GHz-swept optical source realized by injection-locking technique and cascaded FWM process," *Opt. Exp.*, vol. 25, no. 4, pp. 3514–3524, Feb. 2017.
[36] U. Glombitza and E. Brinkmeyer, "Coherent frequency-domain reflectometry for characterization of single-mode integrated-optical waveguides," *J. Lightw. Technol.*, vol. 11, no. 8, pp. 1377–1384, Aug. 1993.
[37] B. J. Soller, D. K. Gifford, M. S. Wolfe, and M. E. Froggatt, "High resolution optical frequency domain reflectometry for characterization of components and assemblies," *Opt. Exp.*, vol. 13, no. 2, pp. 666–674, 2005.
[38] K. Iiyama, "Extended-range high-resolution FMCW reflectometry by means of electronically frequency-multiplied sampling signal generated from auxiliary interferometer," *IEICE Trans. Electron.*, vol. E89-C, no. 6, pp. 823–829, Jun. 2006.
[39] D. Y. Kim, J. Y. Lee, and T. J. Ahn, "Suppression of nonlinear frequency sweep in an optical frequency-domain reflectometer by use of Hilbert transformation," *Appl. Opt.*, vol. 44, no. 35, pp. 7630–7634, 2005.
[40] J. Song, W. Li, P. Lu, Y. Xu, L. Chen, and X. Bao, "Long-range high spatial resolution distributed temperature and strain sensing based on optical frequency-domain reflectometry," *IEEE Photon. J.*, vol. 6, no. 3, pp. 1–8, Jun. 2014.
[41] S. Vergnole, D. Lévesque, and G. Lamouche, "Experimental validation of an optimized signal processing method to handle non-linearity in swept-source optical coherence tomography," *Opt. Exp.*, vol. 18, no. 10, pp. 10361–10446, May 2010.
[42] Z. Ding, T. Liu, Z. Meng, K. Liu, Q. Chen, Y. Du, D. Li, and X. S. Yao, "Note: Improving spatial resolution of optical frequency-domain reflectometry against frequency tuning nonlinearity using non-uniform fast Fourier transform," *Rev. Sci. Instrum.*, vol. 83, no. 6, Jun. 2012, Art. no. 066110.
[43] F. Ito, X. Fan, and Y. Koshikiya, "Long-range coherent OFDR with light source phase noise compensation," *J. Lightw. Technol.*, vol. 30, no. 8, pp. 1015–1024, Apr. 2012.
[44] X. Fan, Y. Koshikiya, and F. Ito, "Phase-noise-compensated optical frequency-domain reflectometry," *IEEE J. Quantum Electron.*, vol. 45, no. 6, pp. 594–602, Jun. 2009.
[45] Z. Ding, Y. Du, T. Liu, X. S. Yao, B. Feng, K. Liu, and J. Jiang, "Long-range high spatial resolution optical frequency-domain reflectometry based on optimized deskew filter method," *Proc. SPIE*, vol. 9274, Nov. 2014, Art. no. 927407.
[46] A. Meta, P. Hoogeboom, and L. Ligthart, "Range non-linearities correction in FMCW SAR," in *Proc. IEEE Int. Symp. Geosci. Remote Sens.*, Jul. 2006, pp. 403–406.
[47] M. Burgos-Garcia, C. Castillo, S. Llorente, J. M. Pardo, and J. C. Crespo, "Digital on-line compensation of errors induced by linear distortion in broadband LFM radars," *Electron. Lett.*, vol. 39, no. 1, pp. 116–118, Jan. 2003.
[48] D. Arbel and A. Eyal, "Dynamic optical frequency domain reflectometry," *Opt. Exp.*, vol. 22, no. 8, pp. 8823–8830, Apr. 2014.
[49] J. Geng, C. Spiegelberg, and S. Jiang, "Narrow linewidth fiber laser for 100-km optical frequency domain reflectometry," *IEEE Photon. Technol. Lett.*, vol. 17, no. 9, pp. 1827–1829, Sep. 2005.
[50] Z. Ding, X. S. Yao, T. Liu, Y. Du, K. Liu, Q. Han, Z. Meng, J. Jiang, and H. Chen, "Long measurement range OFDR beyond laser coherence length," *IEEE Photon. Technol. Lett.*, vol. 25, no. 2, pp. 202–205, Jan. 2013.
[51] L. Shiloh and A. Eyal, "Distributed acoustic and vibration sensing via optical fractional Fourier transform reflectometry," *Opt. Exp.*, vol. 23, no. 4, p. 4296, Feb. 2015.
[52] C. Baker, Y. Lu, J.-I. Song, and X. Bao, "Incoherent optical frequency domain reflectometry based on a Kerr phase-interrogator," *Opt. Exp.*, vol. 22, no. 13, pp. 15370–15375, Jun. 2014.
[53] Q. Liu, X. Fan, and Z. He, "Time-gated digital optical frequency domain reflectometry with 16-m spatial resolution over entire 110-km range," *Opt. Exp.*, vol. 23, no. 20, pp. 25988–25995, Oct. 2015.
[54] S. Wang, X. Fan, Q. Liu, and Z. He, "Distributed fiber-optic vibration sensing based on phase extraction from time-gated digital OFDR," *Opt. Exp.*, vol. 23, no. 26, pp. 33301–33309, 2015.
[55] X. Fan, Y. Koshikiya, and F. Ito, "Centimeter-level spatial resolution over 40 km realized by bandwidth-division phase-noise-compensated OFDR," *Opt. Exp.*, vol. 19, no. 20, pp. 19122–19128, 2011.
[56] Z. Ding, X. Steve Yao, T. Liu, Y. Du, K. Liu, Q. Han, Z. Meng, and D. Li, "Note: Reducing polarization induced sidebands in Rayleigh backscattering spectra for accurate distributed strain measurement using optical frequency-domain reflectometry," *Rev. Sci. Instrum.*, vol. 84, no. 2, Feb. 2013, Art. no. 026101.
[57] C. Shao, G. Yin, L. Lv, M. Liu, I. P. Ikechukwu, H. Han, L. Zhou, J. Zhang, W. Zhai, S. Wang, and T. Zhu, "OFDR with local spectrum matching method for optical fiber shape sensing," *Appl. Phys. Exp.*, vol. 12, no. 8, Jul. 2019, Art. no. 082010.
[58] S. Zhao, J. Cui, L. Suo, Z. Wu, D.-P. Zhou, and J. Tan, "Performance investigation of OFDR sensing system with a wide strain measurement range," *J. Lightw. Technol.*, vol. 37, no. 15, pp. 3721–3727, Aug. 1, 2019.
[59] M. Luo, J. Liu, C. Tang, X. Wang, T. Lan, and B. Kan, "0.5 mm spatial resolution distributed fiber temperature and strain sensor with position-deviation compensation based on OFDR," *Opt. Exp.*, vol. 27, no. 24, pp. 35823–35829, Nov. 2019.
[60] N. Riesen, T. T. Y. Lam, and J. H. Chow, "Resolving the range ambiguity in OFDR using digital signal processing," *Meas. Sci. Technol.*, vol. 25, no. 12, pp. 1–6, Dec. 2014.
[61] N. Riesen, T. T. Y. Lam, and J. H. Chow, "Bandwidth-division in digitally enhanced optical frequency domain reflectometry," *Opt. Exp.*, vol. 21, no. 4, pp. 4017–4026, Feb. 2013.
[62] Y. Kim, M. J. Kim, B. S. Rho, and Y. H. Kim, "Measurement range enhancement of Rayleigh-based optical frequency domain reflectometry with bidirectional determination," *IEEE Photon. J.*, vol. 9, no. 6, pp. 1–8, Dec. 2017.
[63] M. J. Kim, Y. H. Kim, E. Jung, W.-J. Lee, S. H. Hwang, and B. Rho, "Simulation result for dynamic range extension in coherent optical frequency domain reflectometry," in *Proc. Numer. Simulation Optoelectron. Devices*, Palma de Mallorca, Spain, Sep. 2014, pp. 107–108.
[64] L. Suo, Z. Lei, S. Zhao, Z. Wu, and A. Takezawa, "Study on sliding-window length based on Rayleigh backscattering spectrum correlation in distributed optical-fiber strain measurement," *Opt. Fiber Technol.*, vol. 47, pp. 126–132, Jan. 2019.
[65] J. Cui, Z. Shiyuan, D. Yang, and Z. Ding, "Investigation of the interpolation method to improve the distributed strain measurement accuracy in optical frequency domain reflectometry systems," *Appl. Opt.*, vol. 57, no. 6, pp. 1424–1431, Feb. 2018.
[66] K. Feng, J. Cui, H. Dang, X. Sun, D. Jiang, Y. Jin, Y. Niu, and X. Zhang, "Investigation of a signal demodulation method based on wavelet transformation for OFDR to enhance its distributed sensing performance," *Sensors*, vol. 19, no. 13, pp. 1–15, Jul. 2019.
[67] S. Zhao, J. Cui, Z. Wu, and J. Tan, "Accuracy improvement in OFDR-based distributed sensing system by image processing," *Opt. Lasers Eng.*, vol. 124, Jan. 2020, Art. no. 105824.

[68] Y. Park, T.-J. Ahn, J.-C. Kieffer, and J. Azaña, "Optical frequency domain reflectometry based on real-time Fourier transformation," *Opt. Exp.*, vol. 15, no. 8, pp. 4597–4616, Apr. 2007.
[69] A. Malacarne, Y. Park, M. Li, S. LaRochelle, and J. Azana, "Real-time Fourier transformation of lightwave spectra and application in optical reflectometry," *Opt. Exp.*, vol. 23, no. 25, pp. 32516–32527, Dec. 2015.
[70] C. Ma, Q. Zhou, J. Qin, W. Xie, Y. Dong, and W. Hu, "Fast spectrum analysis for an OFDR using the FFT and SCZT combination approach," *IEEE Photon. Technol. Lett.*, vol. 28, no. 6, pp. 657–660, Mar. 15, 2016.
[71] D. Wada, H. Igawa, H. Murayama, and T. Kasai, "Signal processing method based on group delay calculation for distributed Bragg wavelength shift in optical frequency domain reflectometry," *Opt. Exp.*, vol. 22, no. 6, pp. 6829–6836, Mar. 2014.
[72] M. Zhu and H. Murayama, "Fast demodulation of OFDR based long length FBG sensing system for noisy signals," *Opt. Exp.*, vol. 26, no. 16, pp. 19804–19814, Aug. 2018.
[73] Y. Koshikiya, X. Fan, and F. Ito, "Influence of acoustic perturbation of fibers in phase-noise-compensated optical-frequency-domain reflectometry," *J. Lightw. Technol.*, vol. 28, no. 22, pp. 3323–3328, Nov. 2010.
[74] A. Bergman, R. Davidi, A. I. Shalev, L. Ovadia, T. Langer, and M. Tur, "Increasing the measurement dynamic range of Rayleigh-based OFDR interrogator using an amplifying add-on module," *IEEE Photon. Technol. Lett.*, vol. 28, no. 22, pp. 2621–2624, Nov. 15, 2016.
[75] H. Gabai, Y. Botsev, M. Hahami, and A. Eyal, "Optical frequency domain reflectometry at maximum update rate using I/Q detection," *Opt. Lett.*, vol. 40, no. 8, pp. 1725–1728, Apr. 2015.
[76] D.-P. Zhou, Z. Qin, W. Li, L. Chen, and X. Bao, "Distributed vibration sensing with time-resolved optical frequency-domain reflectometry," *Opt. Exp.*, vol. 20, no. 12, pp. 13138–13145, Jun. 2012.
[77] A. K. Sang, M. E. Froggatt, D. K. Gifford, and B. D. Dickerson, "One centimeter spatial resolution temperature measurements from 25 to 850°C using Rayleigh scatter in gold coated fiber," in *Proc. Conf. Lasers Electro-Optics (CLEO)*, May 2007, pp. 1–2.
[78] C. D. Boyd, B. Dickerson, and B. K. Fitzpatrick, "Monitoring distributed temperatures along superconducting degaussing cables via Rayleigh backscattering in optical fibers," in *Proc. Intell. Ships Symp. IX*, Philadelphia, PA, USA, May 2011, pp. 25–26.
[79] C. D. Boyd, E. M. Lally, E. E. Horrell, and B. D. Dickerson, "Verifying cryogenic cooling of superconducting cables using optical fiber," in *Proc. Future Instrum. Int. Workshop (FIIW)*, Oct. 2012, pp. 1–4.
[80] M. E. Froggatt, D. K. Gifford, S. T. Kreger, M. S. Wolfe, and B. J. Soller, "Distributed strain and temperature discrimination in unaltered polarization maintaining fiber," in *Proc. Opt. Fiber Sensors*, 2006, pp. 1–4.
[81] M. E. Froggatt, "Distributed strain and temperature discrimination in polarization maintaining fiber," U.S. Patent 7 538 883, May 26, 2009.
[82] W. Li, L. Chen, and X. Bao, "Compensation of temperature and strain coefficients due to local birefringence using optical frequency domain reflectometry," *Opt. Commun.*, vol. 311, pp. 26–32, Jan. 2013.
[83] D.-P. Zhou, W. Li, L. Chen, and X. Bao, "Distributed temperature and strain discrimination with stimulated Brillouin scattering and Rayleigh backscatter in an optical fiber," *Sensors*, vol. 13, no. 2, pp. 1836–1845, Jan. 2013.
[84] Z. Ding, D. Yang, Y. Du, K. Liu, Y. Zhou, R. Zhang, Z. Xu, J. Jiang, and T. Liu, "Distributed strain and temperature discrimination using two types of fiber in OFDR," *IEEE Photon. J.*, vol. 8, no. 5, pp. 1–8, Oct. 2016.
[85] Z. Ding, X. S. Yao, T. Liu, Y. Du, K. Liu, Q. Han, Z. Meng, and H. Chen, "Long-range vibration sensor based on correlation analysis of optical frequency-domain reflectometry signals," *Opt. Exp.*, vol. 20, no. 27, p. 28319, Dec. 2012.
[86] T. Liu, Y. Du, Z. Ding, K. Liu, Y. Zhou, and J. Jiang, "40-km OFDR-based distributed disturbance optical fiber sensor," *IEEE Photon. Technol. Lett.*, vol. 28, no. 7, pp. 771–774, Apr. 1, 2016.
[87] Z. Ding, D. Yang, K. Liu, J. Jiang, Y. Du, B. Li, M. Shang, and T. Liu, "Long-range OFDR-based distributed vibration optical fiber sensor by multicharacteristics of Rayleigh scattering," *IEEE Photon. J.*, vol. 9, no. 5, pp. 1–10, Oct. 2017.
[88] I. Steinberg, L. Shiloh, H. Gabai, and A. Eyal, "Over 100km long ultra-sensitive dynamic sensing via gated-OFDR," *Proc. SPIE*, vol. 9634, Sep. 2015, Art. no. 96341B.
[89] L. Schenato, R. Aneesh, L. Palmieri, A. Galtarossa, and A. Pasuto, "Fiber optic sensor for hydrostatic pressure and temperature measurement in riverbanks monitoring," *Opt. Laser Technol.*, vol. 82, pp. 57–62, Aug. 2016.
[90] C. Wei, H. Chen, X. Chen, D. Chen, Z. Li, and X. S. Yao, "Distributed transverse stress measurement along an optic fiber using polarimetric OFDR," *Opt. Lett.*, vol. 41, no. 12, pp. 2819–2822, Jun. 2016.
[91] L. Palmieri, D. Sarchi, and A. Galtarossa, "Distributed measurement of high electric current by means of polarimetric optical fiber sensor," *Opt. Exp.*, vol. 23, no. 9, pp. 11073–11079, Apr. 2015.
[92] Y. Du, T. Liu, Z. Ding, K. Liu, B. Feng, and J. Jiang, "Distributed magnetic field sensor based on magnetostriction using Rayleigh backscattering spectra shift in optical frequency-domain reflectometry," *Appl. Phys. Exp.*, vol. 8, no. 1, Jan. 2015, Art. no. 012401, doi: 10.7567/APEX.8.012401.
[93] Y. Du, S. Jothibasu, Y. Zhuang, C. Zhu, and J. Huang, "Rayleigh backscattering based macrobending single mode fiber for distributed refractive index sensing," *Sens. Actuators B, Chem.*, vol. 248, pp. 346–350, Sep. 2017.
[94] A. V. Faustov, A. V. Gusarov, P. Mégret, M. Wuilpart, A. V. Zhukov, S. G. Novikov, V. V. Svetukhin, and A. A. Fotiadi, "The use of optical frequency-domain reflectometry in remote distributed measurements of the $\gamma$-radiation dose," *Tech. Phys. Lett.*, vol. 41, no. 5, pp. 414–417, May 2015.
[95] T. Chen, Q. Wang, R. Chen, B. Zhang, K. P. Chen, M. Maklad, and P. R. Swinehart, "Distributed hydrogen sensing using in-fiber Rayleigh scattering," *Appl. Phys. Lett.*, vol. 100, no. 19, May 2012, Art. no. 191105.
[96] T. Chen, Q. Q. Wang, B. T. Zhang, R. Z. Chen, and K. P. Chen, "Distributed flow sensing using optical hot -wire grid," *Opt. Exp.*, vol. 20, no. 8, pp. 8240–8249, Apr. 2012.
[97] R. G. Duncan, M. E. Froggatt, S. T. Kreger, R. J. Seeley, D. K. Gifford, A. K. Sang, and M. S. abd Wolfe, "High-accuracy fiber-optic shape sensing," *Proc. SPIE*, vol. 6530, Apr. 2007, Art. no. 65301S.
[98] M. E. Froggatt and R. G. Duncan, "Fiber optic position and/or shape sensing based on rayleigh scatter," U.S. Patent, 7 772 541, Aug. 10, 2010.
[99] F. Parent, S. Loranger, K. K. Mandal, V. L. Iezzi, J. Lapointe, J.-S. Boisvert, M. D. Baiad, S. Kadoury, and R. Kashyap, "Enhancement of accuracy in shape sensing of surgical needles using optical frequency domain reflectometry in optical fibers," *Biomed. Opt. Exp.*, vol. 8, no. 4, pp. 2210–2221, 2017.
[100] S. Loranger, M. Gagné, V. Lambin-Iezzi, and R. Kashyap, "Rayleigh scatter based order of magnitude increase in distributed temperature and strain sensing by simple UV exposure of optical fibre," *Sci. Rep.*, vol. 5, no. 1, pp. 1–7, Jun. 2015.
[101] A. Yan, S. Huang, S. Li, R. Chen, P. Ohodnicki, M. Buric, S. Lee, M.-J. Li, and K. P. Chen, "Distributed optical fiber sensors with ultrafast laser enhanced Rayleigh backscattering profiles for real-time monitoring of solid oxide fuel cell operations," *Sci. Rep.*, vol. 7, no. 1, pp. 1–9, Aug. 2017.
[102] S. T. Kreger, A. K. Sang, D. K. Gifford, and M. E. Froggatt, "Distributed strain and temperature sensing in plastic optical fiber using Rayleigh scatter," *Proc. SPIE*, vol. 7316, Apr. 2009, Art. no. 73160A.
[103] S. Rizzolo, A. Boukenter, J. Perisse, G. Bouwmans, H. El Hamzaoui, L. Bigot, Y. Ouerdane, M. Cannas, M. Bouazaoui, J.-R. Mace, S. Bauer, and S. Girard, "Radiation response of OFDR distributed sensors based on microstructured pure silica optical fibers," in *Proc. 15th Eur. Conf. Radiat. Effects Compon. Syst. (RADECS)*, Sep. 2015, pp. 1–3.
[104] M. Morshed, M. I. Hassan, T. K. Roy, M. S. Uddin, and S. M. A. Razzak, "Microstructure core photonic crystal fiber for gas sensing applications," *Appl. Opt.*, vol. 54, no. 29, pp. 8637–8643, Oct. 2015.

**CHANGSHUO LIANG** received the B.Sc. degree from Northeastern University, China, in 2017. He is currently pursuing the M.Eng. degree with the Taiyuan University of Technology. His main research interest includes optical fiber sensors.

**QING BAI** received the Ph.D. degree in physical electronics from the Taiyuan University of Technology, in 2019. He is currently an Assistant Research Fellow with the Key Laboratory of Advanced Transducers and Intelligent Control System, Taiyuan University of Technology. His current research interests include optical fiber sensors and engineering application.

**MIN YAN** received the B.Sc. degree from the North University of China, China, in 2018. She is currently pursuing the M.Eng. degree with the Taiyuan University of Technology. Her main research interest includes optical fiber sensors.

**YU WANG** received the Ph.D. degree in electrical and electronic engineering from the University of Cergy-Pontoise, France, in 2014. He is currently an Associate Professor with the Key Laboratory of Advanced Transducers and Intelligent Control System, Taiyuan University of Technology, and Science and Technology on Near-Surface Detection Laboratory. His current research interests include vibration detection and optical fiber sensors.

**HONGJUAN ZHANG** received the Ph.D. degree from the Taiyuan University of Technology, China, in 2011. She is currently a Professor with the College of Electrical and Power Engineering, Taiyuan University of Technology. Her research interests include new sensor technology and power electronics conversion control technology.

**BAOQUAN JIN** received the Ph.D. degree in mechatronic engineering from the Taiyuan University of Technology, in 2010. He is currently a Professor with the Key Laboratory of Advanced Transducers and Intelligent Control System, and the State Key Laboratory of Coal and CBM Co-mining. His research interests include sensors, optical fiber sensing, and engineering application.